Mechanism of Ubiquinol Oxidation by the bc_1 Complex: Different Domains of the Quinol Binding Pocket and Their Role in the Mechanism and Binding of Inhibitors†

Antony R. Crofts,*,‡ Blanca Barquera,§ Robert B. Gennis,‡,§ Richard Kuras,‡ Mariana Guergova-Kuras,‡ and Edward A. Berry*,||

Center for Biophysics and Computational Biology and Department of Biochemistry, University of Illinois at Urbana−Champaign, Urbana, Illinois 61801, and Lawrence Berkeley National Laboratory, University of California, Berkeley, California 94720

Received April 27, 1999; Revised Manuscript Received August 16, 1999

ABSTRACT: Structures of mitochondrial ubihydroquinone:cytochrome *c* oxidoreductase (bc_1 complex) from several animal sources have provided a basis for understanding the functional mechanism at the molecular level. Using structures of the chicken complex with and without inhibitors, we analyze the effects of mutation on quinol oxidation at the Q_o site of the complex. We suggest a mechanism for the reaction that incorporates two features revealed by the structures, a movement of the iron sulfur protein between two separate reaction domains on cytochrome c_1 and cytochrome *b* and a bifurcated volume for the Q_o site. The volume identified by inhibitor binding as the Q_o site has two domains in which inhibitors of different classes bind differentially; a domain proximal to heme b_L, where myxothiazole and β-methoxyacrylate-(MOA-) type inhibitors bind (class II), and a distal domain close to the iron sulfur protein docking interface, where stigmatellin and 5-*n*-undecyl-6-hydroxy-4,7-dioxobenzothiaole (UHDBT) bind (class I). Displacement of one class of inhibitor by another is accounted for by the overlap of their volumes, since the exit tunnel to the lipid phase forces the hydrophobic "tails" to occupy common space. We conclude that the site can contain only one "tailed" occupant, either an inhibitor or a quinol or one of their reaction products. The differential sensitivity of strains with mutations in the different domains is explained by the proximity of the affected residues to the binding domains of the inhibitors. New insights into mechanism are provided by analysis of mutations that affect changes in the electron paramagnetic resonance (EPR) spectrum of the iron sulfur protein, associated with its interactions with the Q_o-site occupant. The structures show that all interactions with the iron sulfur protein must occur at the distal position. These include interactions between quinone, or class I inhibitors, and the reduced iron sulfur protein and formation of a reaction complex between quinol and oxidized iron sulfur protein. The step with high activation energy is after formation of the reaction complex, likely in formation of the semiquinone and subsequent dissociation of the complex into products. We suggest that further progress of the reaction requires a movement of semiquinone to the proximal position, thus mapping the bifurcated reaction to the bifurcated volume. We suggest that such a movement, together with a change in conformation of the site, would remove any semiquinone formed from further interaction with the oxidized [2Fe-2S] center and also from reaction with O_2 to form superoxide anion. We also identify two separate reaction paths for exit of the two protons released in quinol oxidation.

The ubiquinol:cytochrome *c* oxidoreductases family of enzymes (the bc_1 complexes)[1] are central components of many electron-transfer systems, occurring ubiquitously in respiratory and photosynthetic chains of mitochondria and bacteria and (as the b_6f complex) in the photosynthetic chain of oxygenic photosynthesis (see refs *1*−*6* for recent reviews). The enzyme catalyzes the oxidation of quinol, the reduction of cytochrome *c* (or plastocyanin in chloroplasts), and the electrogenic translocation of protons across the membrane. All bc_1 complexes contain three essential subunits to which the prosthetic groups are bound. These are cytochrome *b*, with one high-potential heme (b_H) and one low-potential heme (b_L), the Rieske iron sulfur protein (ISP) containing a [2Fe-2S] center, and cytochrome (cyt) c_1. Structures for the mitochondrial complex from several vertebrate sources have recently been reported (*7*−*11*), showing as many as 11 subunits. In *Rhodobacter* species the enzyme functions in both respiratory and photosynthetic chains and has a simpler subunit complement. In *Rhodobacter sphaeroides*, when grown under photosynthetic conditions, the three catalytic

† We acknowledge with gratitude the support for this research provided by NIH Grants GM 35438 (to A.R.C.) and DK 44842 (to E.A.B.), and by the Office of Health and Environmental Research, U.S. Department of Energy, under Contract DE-AC03-76SF00098 (to E.A.B.).

* Corresponding authors: for functional aspects, A.R.C., Center for Biophysics and Computational Biology, University of Illinois at Urbana−Champaign, 388 Morrill Hall, 505 S. Goodwin, Urbana, IL 61801; for structural aspects, E.A.B., Structural Biology Division, Lawrence Berkeley National Laboratory, 250 Melvyn Calvin Lab 5230, University of California, Berkeley, CA 94720-5230.

‡ Center for Biophysics and Computational Biology, University of Illinois.

§ Department of Biochemistry, University of Illinois.

|| University of California.

10.1021/bi990962m CCC: $18.00
Published on Web 11/05/1999

subunits, and a fourth subunit of unknown function, are present (*12*, *13*). The functions of many of the supernumerary mitochondrial subunits are not well understood, but they are not thought to have a direct role in catalysis. The crystallographic structures have provided a new perspective on the relation between structure and function.

The catalytic mechanism of the bc_1 complex has been extensively studied. Much of the mechanistic work has been done in photosynthetic bacteria, where the option of flash excitation provides a greater experimental flexibility, and molecular engineering protocols have allowed exploration of function through specific mutagenesis. A modified Q cycle (*1*−*3*, *6*, *14*−*21*) accounts well for the experimental data. Quinol is oxidized at the Q_o site of the complex in a reaction with a relatively high activation barrier (*21*). One electron is transferred to a high-potential chain and the other to a low-potential chain, in the so-called bifurcated reaction. The high-potential chain, consisting of the ISP, cyt c_1, and cyt *c* (or c_2), transfers the first electron from quinol to an acceptor (cytochrome oxidase in mitochondria, the oxidized photochemical reaction center in photosynthetic systems). Because QH_2 oxidation is the limiting step and proceeds through a high activation barrier, the reaction at the Q_o site appears to be a concerted electron transfer to the high- and low-potential chains. It is generally supposed that an intermediate semiquinone is generated at the Q_o site, but this has not been detected (*21*, *22*). The low-potential chain consists of two cyt *b* hemes, which form a pathway through which electrons are transferred across the coupling membrane from the Q_o site to the Q_i site. To provide the two electrons at the Q_i site required for reduction of quinone, the Q_o site oxidizes 2 equiv of quinol in successive turnovers (*15*). The first electron at the Q_i site generates a relatively stable semiquinone that is reduced to quinol by the second electron. The overall reaction generates four protons in the periplasmic space (the side of *p*ositive protonic potential, or P side), and the formation of quinol uses up two protons from the cytoplasmic side (the N side, of *n*egative protonic potential). Bifurcation of the reaction at the Q_o site is essential for proton pumping and for conservation of the free energy released in the reaction, and occurs with high stoichiometric efficiency:

$$QH_2 + 2\ \text{cyt}\ c^{3+} + 2H^+_N \Leftrightarrow Q + 2\ \text{cyt}\ c^{2+} + 4H^+_P$$

[1] Abbreviations: bc_1 complex, ubihydroquinone:cytochrome *c* oxidoreductase; b_H, higher potential cytochrome *b* heme; b_L, lower potential cytochrome *b* heme; cyt, cytochrome; EPR, electron paramagnetic resonance; [2Fe-2S] or Fe_2S_2, iron sulfur cluster of the Rieske-type iron sulfur protein; ISP, Rieske-type iron sulfur protein; ISP^{ox} and ISP^{red}, oxidized and reduced states of the iron sulfur protein; ISP_B or ISP_C, iron sulfur protein docked at cytochrome *b* or cytochrome c_1 interface, respectively; MOA, *β*-methoxyacrylate, or similar group, acting as the pharmacophore of a class of inhibitors of the Q_o site; Q, ubiquinone or quinone; $Q^{\bullet -}$, ubisemiquinone anion; Q_A, ubiquinone bound in the primary acceptor quinone pocket of the bacterial reaction center; Q_B, ubiquinone bound in the secondary acceptor quinone pocket of the bacterial reaction center; $QH^\bullet$, ubisemiquinone, neutral form; QH_2, ubihydroquinone or quinol; QH^-, ubihydroquinone anion; Q_i site, quinone reducing site; Q_o site, quinol oxidizing site; Q_i or Q_iH_2, ubiquinone or ubihydroquinone at the Q_i site; Q_o, Q_oH_2, ubiquinone or ubihydroquinone at the Q_o site; Q_{os} and Q_{ow}, strongly and weakly binding quinone molecules bound to the Q_o site; -PEWY-, highly conserved span of cytochrome *b* with this sequence in single-letter amino acid code; SQ, ubisemiquinone (protonation state unspecified); UHDBT, 5-*n*-undecyl-6-hydroxy-4,7-dioxobenzothiazole; UHNQ, 3-undecyl-2-hydroxy-1,4-naphthoquinone.

Inhibitors at the Q_o site fall into two main classes (*23*−*30*). UHDBT and stigmatellin (class I) interact specifically with the [2Fe-2S] center, perturbing its spectroscopic and redox properties, and prevent its oxidation by cyt c_1 (*23*−*26*). Myxothiazole and MOA-type inhibitors (class II) do not interact with the [2Fe-2S] center but shift the spectrum of heme b_L (*27*−*29*). Binding studies have demonstrated that occupation by inhibitors is mutually exclusive (*23*−*29*), and the crystallographic studies have shown that stigmatellin, UHDBT, myxothiazole, and MOA-stilbene occupy an overlapping volume (*7*−*11*). Further information on the occupancy of the Q_o site has been obtained though study of the interaction of the occupant with the [2Fe-2S] center of the reduced ISP, observed through changes in the EPR spectrum. In addition to the effects observed with stigmatellin and UHDBT (*23*−*26*), a well-defined spectral change giving rise to a band at $g_x = 1.80$ has been characterized when quinone and the reduced ISP are both present (*31*−*37*). The dependence on ambient redox potential, and on the extent of extraction of quinone, has lead Ding and colleagues to suggest a double occupancy of the site by weakly (Q_{ow}) and strongly (Q_{os}) binding quinone species (*34*−*37*). Inhibitors of either class eliminate EPR signals ascribed to both species (*34*, *35*). Support for occupancy of the Q_o site by more than one species has been suggested by Brandt et al. (*30*) on the basis of kinetic studies interpreted as showing noncompetitive binding of MOA-type inhibitors in the presence of substrate quinol.

Although the modified Q-cycle mechanism is well supported, there remain several problems in understanding the mechanism of catalysis at the molecular level. Most significant is the paradox of the bifurcated reaction. The semiquinone intermediate formed in quinol oxidation must have a low enough potential to reduce cyt b_L but does not react with the oxidized ISP at a significant rate, despite the strong thermodynamic gradient favoring this reaction. A more detailed understanding of the structure−function relationship at the catalytic sites requires a structural context, and this has now been provided by X-ray crystallographic studies (*7*−*10*). The structures have already revealed a hitherto unsuspected complexity in the reaction mechanism. The extrinsic head of the ISP serves as a mobile domain, ferrying redox equivalents between reaction interfaces on cyt c_1 and cyt *b* through a 22 Å movement (*7*, *11*, *38*−*40*).

In this paper, we present details of the structures of the chicken heart mitochondrial bc_1 complex in the native state and in cocrystals with inhibitors (*7*), as these pertain to operation of the Q_o site.The structures show no evidence for occupancy of the Q_o site by more than one species. In the context of the structures, we discuss studies of function in strains in which mutation affects the Q_o site. We discuss the pathways by which protons are released, and we propose a mechanism based on single occupancy for the site that fits the available data and explains how the bifurcated reaction works. Preliminary accounts of some of this work have appeared elsewhere (*7*, *11*, *40*−*43*).

METHODS AND MATERIALS

Crystallographic Methods. The crystallographic determination of the structures of the complex from chicken heart mitochondria has been discussed at length elsewhere (*7*).

Coordinate data sets have been deposited in the Brookhaven Protein Data Bank as files 1bcc (native complex with quinone at Q_i site, lipids, and detergents), 2bcc (complex with stigmatellin), and 3bcc (complex cocrystallized with stigmatellin and antimycin). Refined structures have also been solved at similar resolution for the chicken complexes with myxothiazole or MOA-stilbene bound. Refinement data for all these structures are included in a companion paper (*38*). Additional structures containing other inhibitors including UHDBT, and other MOA-type inhibitors, have been solved and are currently under further refinement (E. A. Berry, and Z. Zhang, unpublished work) but are referred to only briefly in this paper.

Inhibitors were modeled to fit electron densities in separate crystal structures containing each inhibitor. Crystals were grown in the presence of inhibitors at saturating concentrations, as detailed previously (*7*). At the present resolution, the positions of individual atoms are not resolved, so atomic structures shown should be regarded as preliminary.

Graphic representation of the structures was realized by use of Chime [Molecular Design Limited (MDL), Chemscape Chime, version 2.0.3), a plug-in for the Netscape browser (Netscape Communicator, version 4.04). Surfaces were calculated by using the *surface* function of Chime, with a 1.4 Å probe.

Molecular Engineering Protocols. Molecular engineering of cyt *b* of *Rb. sphaeroides* was performed as previously described (*44*), and specific plasmids and protocols will be described in detail elsewhere. Kinetic characterization of mutant strains (*15*−*19*, *21*) and characterization of interactions between quinone and the ISP by EPR (*34*) used established protocols, and experimental details will be also be given separately.

Computer Models. Homology modeling was carried out with the module Modeller (*45*) in the CHARMm package of programs (Molecular Simulations Inc.). The energy minimization to eliminate improper atomic overlaps and poor geometry was performed with CHARMm/X-PLOR running on an SGI Indigo2 computer. During preliminary minimization, backbone atoms of conserved residues were constrained. The coordinate bonds of prosthetic groups and the metal−ligand bonds were held constant by distance constraints at all stages of energy minimization. Modeling of the quinones at the Q_o site was performed with SCULPT (*46*) (Interactive Simulations Inc.) running on a PC computer. After removal of the coordinate data for the incumbent inhibitor, the quinone abstracted from file 4rcr (photochemical reaction center) was positioned at the Q_o site to mimic the inhibitor. For occupancy of the distal domain, the protein (stigmatellin-containing structure) was frozen, and, after preliminary position to replace the inhibitor, the quinone was tethered to the His-161 and Glu-272 and then relaxed with SCULPT, to eliminate van der Waals overlap and to minimize the global free energy. This positioned the quinone symmetrically between the two ligands, with a distance appropriate for H-bonding, and in conformation with the stigmatellin volume. Two H-atoms were added to convert the model to a quinol. For occupancy of the proximal domain, the quinone ring was positioned to replace the inhibitor in the myxothiazole-containing structure, so as to match approximately the position of the pharmacophore, and then relaxed while the protein was kept frozen. In this position, the quinone was constrained to the volume available to myxothiazole. The [2Fe-2S] cluster, the heme, and their ligands were frozen during the energy minimization. Water molecules in the putative water chain were based on the data of ref *47*, with some relaxation to accommodate residue changes in different structures.

RESULTS

Structure of the Q_o Site. The structural studies (*7*−*10*) have confirmed the general features anticipated from sequence analysis, structural prediction, biochemical and biophysical studies, and the position of residue changes leading to inhibitor resistance (*1*, *3*, *5*, *48*) and have provided a wealth of additional detail. Spans in the sequence predicted to contribute to the function are highlighted in Figure 1(top), which shows a ribbon representation of the Q_o site of one functional monomer from the chicken heart mitochondrial bc_1 complex. The structure is from 2bcc, which contains stigmatellin bound at the site. Superimposed on the stigmatellin structure are models of myxothiazole and MOA-stilbene, to show the general features of the common volume and the overlap. Residues at which mutagenesis leads to inhibitor resistance or introduces changes in function at the Q_o site are shown as stick models, to indicate their location relative to the site.

Sequence similarity across the bacterial/mitochondrial evolutionary divide shows a strong conservation, so the three subunits may be taken as representative of the catalytic core of the complex from *Rhodobacter* species, where much of the molecular engineering and kinetic characterization has been done. We have constructed homology models of the three catalytic subunits, using the *Rb. sphaeroides* sequence, with the structure of the catalytic subunits from the chicken heart mitochondrial complex as a template. In aspects of the structure relevant to this paper, the homology models followed closely the mitochondrial structure, and we have chosen to use the latter for discussion, since that is the primary structural data. Aligned sequences of cyt *b* from diverse species are shown in Figure 2, annotated to show the structural features referred to in the discussion below and the architectural roles of conserved residues.

The site is defined by three major features:

(i) The first feature is a concave, exterior-facing surface, which provides the docking interface for the ISP, shown by the [2Fe-2S] center, and His-161. The surface is highly conserved (*38*; see alignment in Figure 2) and contains at its apex in the stigmatellin-containing structure an opening between the distal lobe of the Q_o site and the exterior, through which His-161 contacts the inhibitor. This docking interface is discussed in greater detail in a companion paper (*38*).

(ii) The second feature is a bifurcated volume in which electron density is seen in crystals containing myxothiazole, MOA-type inhibitors, UHDBT, or stigmatellin (Figures 1 and 3). From their known action at the site, their occupancy defines this as the quinol binding pocket. The volume is formed by the following spans: the C-terminal end of helix C (shown in blue in Figure 1, top), the connecting loop to the cd1 amphipathic helix (in green-blue), the ef loop, including a coil from the end of the helix E (in green), the -PEWY- turn (in yellow), the short ef helix (in orange)

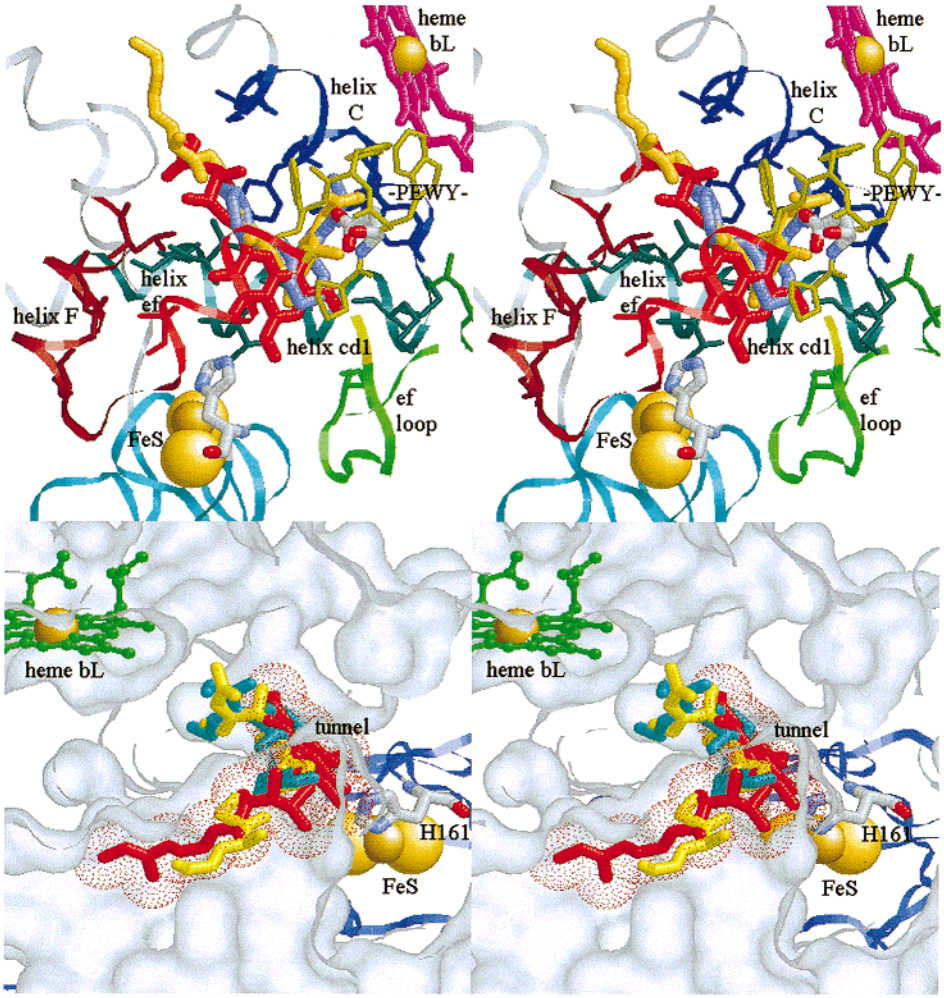

FIGURE 1: Overview of the Q_o site in the stigmatellin-containing structure. (Top) The bc_1 complex is shown as a ribbon structure, with cyt *b* in gray, but the spans contributing to the site are colored as follows: helix C, in blue; the connecting loop to the cd1 amphipathic helix, in green-blue; a coil from the end of helix E, in green; the ef loop, including the -PEWY- turn, in yellow; the small ef helix connecting the -PEWY- turn to transmembrane helix, in orange; and the N-terminal end of helix F, in red. Most of the rest of cyt *b* has been cut away to reveal the site. Residues at which mutation changes the function of the Q_o site are shown as wire-frame models. Heme b_L is shown as a wire-frame model in magenta, with the Fe atom as a space-filling sphere. The ISP is shown by a pale-blue ribbon, with the cluster atoms as space-filling spheres. Ligands to stigmatellin (His-161 of ISP and Glu-272 of cyt *b*) are shown as tubes with CPK coloring. Stigmatellin is shown as a red tubular structure. Models of myxothiazole (orange) and MOA-stilbene (blue), abstracted from separate structures in the same reference orientation, are superimposed on the stigmatellin structure to show the overlap in occupancy. (bottom) Surface of cyt *b* viewed from the lipid phase, looking down the tunnel into the Q_o site pocket. The red dots show the volume of stigmatellin. Stigmatellin is shown as a red tubular structure. Structures for myxothiazole (yellow) and MOA-stilbene (cyan) are superimposed on the stigmatellin structure to show the overlap in occupancy. Heme b_L is shown as a ball-and-stick model in green, with the Fe atom as a space-filling sphere. The ISP is shown as a blue ribbon, with the cluster as space-filling spheres, and with His-161 as a CPK-colored tube. These panels are presented as stereopairs for crossed-eye viewing.

connecting the -PEWY- turn to transmembrane helix, and the N-terminal end of helix F (in dark red). The ends of the transmembrane helices flare out to provide the volume in which the inhibitors bind, and the amphipathic helices and the -PEWY- loop form other bounding walls and the docking interface for the ISP. A tunnel connects the site to the membrane phase. One domain of the bifurcated volume, the proximal lobe, is near heme b_L and is occupied by the pharmacophore side chains of myxothiazole or the MOA-type inhibitors (Figures 1 and 3B,C). The second domain, the distal lobe, is close to the ISP interface, and opens onto it through a hole that is visible when the surface is mapped by a 1.4 Å radius probe. The rings of stigmatellin and UHDBT bind in this volume (Figures 1 and 3A). The tails of all the inhibitors extend toward the membrane phase through the common channel of the tunnel (Figure 1B).

(iii) The third point of note is that the structure of the site brings together spans distant in the sequence. A number of H-bonds involving side chains of conserved residues (Q138−V264, Q138−N261, W142−N261, and W136−A60) hold these together. As discussed below, the site shows considerable expansion upon binding inhibitors, and this loose stitching might facilitate these accommodations.

From the structures of Zhang et al. (*7*), neither the cyt *b* nor the cyt c_1 subunit appears to undergo any large-scale change in structure on binding inhibitors. In contrast, the ISP changes its position dramatically on binding stigmatellin (*7*; see Figure 3C) or UHDBT (*7, 8, 10*). Kim et al. (*10*) noted that, in crystals containing MOA-type inhibitors, density of the [2Fe-2S] cluster was lost from a binding domain near cyt *b*, and we have noted a similar but less marked effect in our structures (*39*). Although there are no

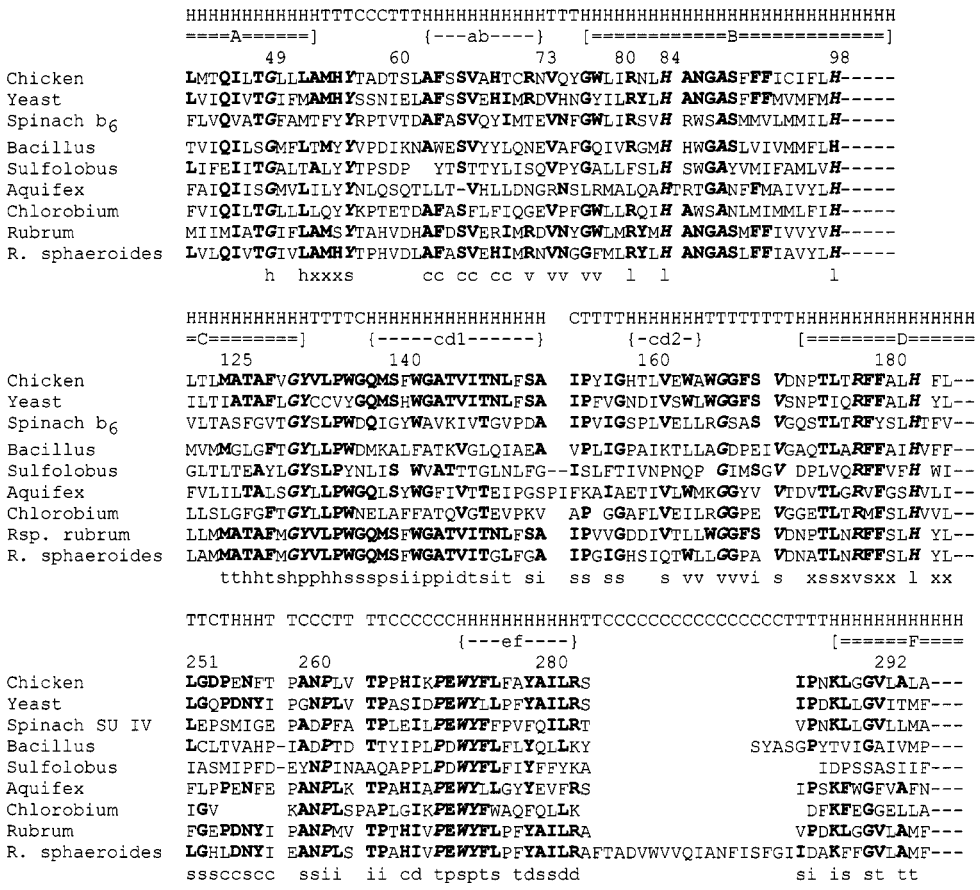

FIGURE 2: Sequences of cyt *b*, cyt b_6, and subunit IV from representative species. Conserved residues are shown in bold-face roman type if conserved within the mitochondrial family and in bold-face italic type if completely conserved. The secondary structure is encoded above the aligned sequences as H (helix), T (turn), E (sheet), or C (coil), and the helices are named as previously suggested (*7*, *8*, *48*). The architectural role of each conserved residue is shown below the alignment by the following code: h, heme contacts, not ligand; l, heme ligand (Fe or propionate); x, dimer contacts; c, monomer contacts to c_1; v, vise for ISP tail; s, structural, within cyt *b* (H-bond stitching or hydrophobic packing); i, ISP interface; t, tunnel from Q_o site to lipid phase (the common volume of occupancy); p, proximal lobe of Q_o site; d, distal lobe of Q_o site and also the opening from the Q_o site onto ISP interface (residues also interface with ISP).

major structural changes in cyt *b* upon binding inhibitors at the Q_o site, there are significant local changes to allow accommodation of the occupant.

The occupancies by stigmatellin, myxothiazole, and MOA-stilbene are illustrated separately in Figure 3, in which cyt *b* is represented by its surface. The protein of cyt *b* has been cut away to reveal the occupants. In Figure 3A, stigmatellin occupies the distal domain. In this position, the distance from the heme b_L is about twice that for the occupants of the proximal domain. In Figure 3B,C, the myxothiazole- and MOA-stilbene-containing structures show the inhibitors with the pharmacophore occupying the proximal domain, close to heme b_L. In these structures, the ISP was close to cyt c_1 and separated from the cyt *b* docking interface by a distinct cleft.

Residues at which mutation affects inhibitor binding at the Q_o site are shown in greater detail in Figure 4. The residues are color-coded to indicate the effect of mutation (*40*). Analysis for inhibitor resistance has not been systematically studied at all sites, and where resistance to one inhibitor has been demonstrated, this does not necessarily mean that other inhibitors have been tested. Mutations at residues shown in yellow lead to resistance to myxothiazole or mucidin (but resistance to stigmatellin has not been reported). Changes at residues shown in red lead to resistance to stigmatellin (but resistance to myxothiazole or mucidin has not been reported). Residues shown in green indicate sites at which resistance to both classes of inhibitor is found.

Stigmatellin-Binding Site. The rings of stigmatellin occupy the end of the pocket distal to heme b_L, and the tail exits the site toward the lipid through the tunnel. The tunnel constrains all occupants so that their volumes overlap in this and in the adjacent space inside the binding pocket. The side chains of M125, E272, A126, and F129 (from the proximal side), P271, F275, I147, L295, and Y279 from the distal side, and A278, which makes no contacts, contribute the surface of this common volume. Stigmatellin binds at a distance of ~11−12 Å from the nearest atom of heme b_L. In the presence of stigmatellin, the ISP is found closely docked at the concave interface. A strong density connection is found between the headgroup of stigmatellin and H161 of the ISP (*7*, *11*, *38*). We have modeled this as a H-bond between Nϵ of H161, and carbonyl and O-methyl groups of stigmatellin. The side chains of L150, I269, L282, R283, Y279, V344, and V146 line the aperture in cyt *b* through which H161 accesses the stigmatellin.

The side chain of Glu-272 of the -PEWY- loop projects into the Q_o pocket in the stigmatellin structures, close enough to H-bond with the OH group of the second ring of the inhibitor (Figure 3A). This configuration was not detected

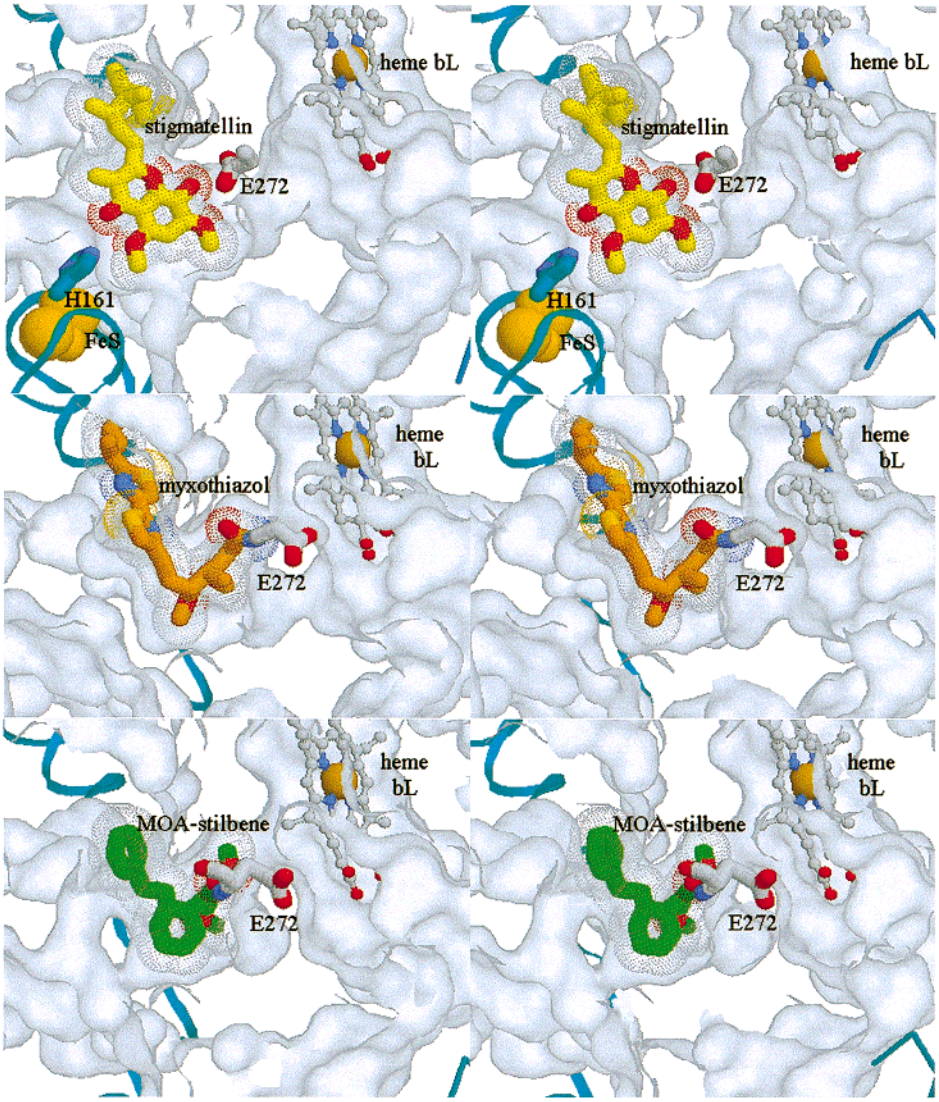

FIGURE 3: Bifurcated volume of the Q_o site, shown by the surfaces of the protein. (A, top) Stigmatellin-containing structure. The surface of the protein (excluding prosthetic groups) was calculated by use of the Chime surface function and colored white. The surface has been cut away to show the Q_o pocket, with stigmatellin (tube model with C atoms shown in yellow) in place, with the ring in the distal domain. The heme b_L (ball-and-stick model shown in CPK colors) is visible at upper right. The [2Fe-2S] cluster (lower left) is shown by spheres, and the ISP is represented by a cyan ribbon, with the side chain of His-161, which provides a ligand to the cluster and also to stigmatellin, shown as a tube model with C atoms in blue. Glu-272, a ligand from cyt *b*, is similarly shown, in CPK coloring. The volume of the inhibitor is shown by the dotted surface. (B, middle), Myxothiazole-containing structure. Coloring is as for panel A, except that myxothiazole is shown as a tube model with C atoms in orange. The pharmacophore group is shown in the proximal domain of the Q_o pocket. The [2Fe-2S] is not visible, because it has rotate to the ISP_C position. (C, bottom) MOA-stilbene-containing structure. Coloring is as for panel B but with the inhibitor with C atoms shown in green.

in previous analyses (3bcc) but emerged from the refinement of 2bcc and has been subsequently confirmed by further refinement of the electron densities for crystals used for 3bcc. In the native structure, and with both proximal-domain inhibitors, the side chain is rotated away from the pocket (Figure 3B,C), so the new configuration in the stigmatellin-containing structures likely represents an important ligand for the distal domain occupant. Strains with mutations at this position in *Rb. sphaeroides* (E295D, -Q, or -G) were resistant to stigmatellin and showed inhibited rates of QH_2 oxidation and a raised K_m (*43*), consistent with this liganding function.

Other residue changes in cyt *b* leading to stigmatellin resistance have been reported at positions M125, F129, G137, I147, T148, N256, W273, V292, and L295 (or equivalent residues in yeast, mouse, *Rhodobacter capsulatus* or *Rhodobacter sphaeroides*) (*1*−*3*, *5*, *43*; and see Figure 4, top). The side chains of M125, F129, I147, and L295 contribute to the surface seen by the inhibitor, and modifications might be expected to change the packing. Several "stigmatellin-resistance" residues seem to play a more structural role, since they do not impinge on the site. G137 and N256 contribute to a polar patch of H-bonded residues, including S140 and the backbone O of Y132, which hold these two spans, distant in sequence, in close apposition to form the site. The side chain of W273 points away from the site to make a H-bond with conserved S89. Conserved T148 is close to the distal lobe but points away from the pocket and forms a part of the lipid-facing surface of the funnel of the quinone access port. V292 is ~8 Å away from the site and also contributes to the funnel surface. It is not obvious how changes at either

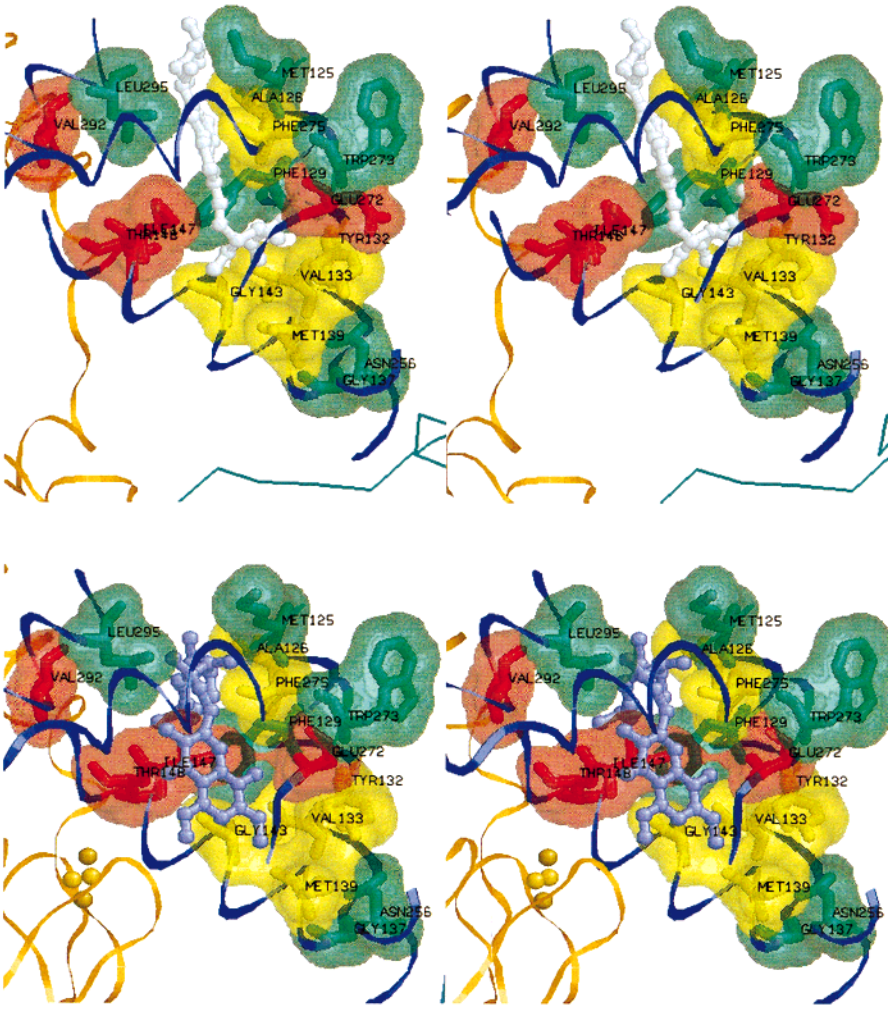

FIGURE 4: Residues at which modification leads to inhibitor resistance. The residues are shown as tube models, numbered at the Cα atom, enclosed by their transparent surfaces to show how they contribute to the binding domains. Myxothiazole-resistant sites are shown in yellow; stigmatellin resistance sites are shown in red. Residues at which modification leads to resistance to both inhibitors are shown in green. Separate structures are shown for the myxothiazole- (top) and stigmatellin- (bottom) containing structures. The inhibitors are shown as ball-and-stick models, colored white and cyan, respectively. The spans of cytochrome *b* contributing to the Q_o site are shown as a blue ribbon. The ISP is shown as an orange ribbon, with the [2Fe-2S] cluster as small orange spheres. Note that, in many cases, several mutations have been generated at a site, with differential effects on inhibitor binding, depending on the nature of the change. The color coding is therefore somewhat simplistic.

of these residues would lead to stigmatellin resistance, unless through specific interactions with the "tail" not yet detected in structures.

Binding Site for Myxothiazole and MOA-Type Inhibitors. Myxothiazole and MOA-stilbene bind in the same cavity as stigmatellin but are displaced ~5.5 Å toward heme b_L and the center of the membrane. In the presence of these class II inhibitors, the position of the ISP was close to cyt c_1, as in the native structure, suggesting that no strong interactions of these inhibitors with the ISP occur, consistent with the lack of redox or spectral change induced by their binding (*24*, *25*, *27*−*29*). Structures with well-defined densities have also been obtained for cocrystals with several iodinated homologues of MOA-type inhibitors, which have aided determination of the orientation of the pharmacophore group (E. A. Berry, and Z. Zhang, unpublished results). For MOA-stilbene, the essential carbonyl oxygen of the MOA-type pharmacophore (*28*) was modeled as forming a weak H-bond with backbone NH of Glu-272 of the -PEWY- loop. The methoxy group of the pharmacophore points to a polar volume including backbone atoms of F129, M139, S140, and V133. The pharmacophore of myxothiazole is not identical to that of the MOA-type inhibitors but could be modeled in a similar configuration. Although myxothiazole or MOA-stilbene is closer to heme b_L than stigmatellin, helix C separates the inhibitor binding pocket from the heme face and from His-183, the ligand to the Fe of heme b_L. This makes it unlikely that this histidine could provide a ligand to the occupant, as previously suggested for ubiquinol (*35*). The heme edge comes forward toward the binding pocket, but there are no contacts between myxothiazole or MOA-type inhibitors and heme b_L.

In both the MOA-stilbene and myxothiazole structures, the side chain of Glu-272 had rotated out of the pocket compared to the stigmatellin structure. This rotation opened the volume for occupation by the pharmacophore side chain, which would otherwise be occluded by overlap. In the "out" position, the side chain pointed away from the binding pocket and toward an exterior cavity that connects to the P phase. The edge of heme b_L with the propionate side chains, with Arg-83, also faces this aqueous cavity, and the polar side chains of E272, Y132, S140, and Y274 contribute to the

exterior surface. On their other sides, these residues also form part of the surface of the proximal domain of the Q_o pocket. Most mutations reported at these residues have led to disrupted function or slowed electron transfer. Although the backbone NH of E272 is modeled as forming a H-bond to MOA-stilbene, mutations at this residue (E295G and E295Q in *Rb. sphaeroides* numbering) led to stigmatellin resistance (*5, 43*) but not resistance to myxothiazole. The side chain presumably plays no role in binding of the class II inhibitors. The backbone configuration of the -PEWY- loop is tightly constrained by H-bonding, which is maintained in each of our structures.

Residues where changes modifying myxothiazole binding but not that of stigmatellin have been reported are A126, Y132, V133, M139, G143, and F275 (Figure 4, bottom). They contribute to the surface of the Q_o site in the proximal domain. The residue equivalent to F275 is leucine in yeast, and a change there to phenylalanine, serine, or threonine gave myxothiazole and mucidin resistance. Sites at which mutation introduced resistance to both myxothiazole and stigmatellin include M125, F129, L295, G137, N256, and W273. The first three impinge on the common surface for both inhibitors; the others have an indirect structural role as discussed above.

Conformational Changes on Binding Inhibitors at the Q_o Site. On binding stigmatellin, the ISP moves from the cyt c_1 interface to an intimate docking on cyt *b*. This allows Nϵ of H161 of the ISP to H-bond to carbonyl and O-methyl O atoms of the inhibitor, to provide the main force constraining the ISP head in this position. Changes in cyt *b* at the ISP docking interface, discussed in detail in a companion paper (*38*), include rotation of Y279, I269, and I147 away from the entrance of the pocket to allow access of ISP His-161 and a repositioning of K288 on the docking surface. This allows the side-chain NH_2 to form a new H-bonding configuration, including contacts to ISP. Deeper in the pocket, the main effect is an enlargement of the volume of the site through a substantial displacement of the -PEWY- loop in one direction and of the cd1 helix in the opposite direction. This widens the volume by ~2.0 Å. As noted above, Glu-272 rotates to point into the binding pocket and form a H-bonds with the OH of stigmatellin. We believe that this rotation is of importance in release of the second proton from the site (*49*). Hydrophobic residues F275, F129, and L282 rotate to accommodate the inhibitor. Although at the present resolution the significance of these changes must be speculative, impaired function on site-directed mutagenesis of each of these residues has demonstrated their importance to function.

Structural changes from the native configuration are also apparent in cocrystals with myxothiazole. In contrast to the stigmatellin structure, the ISP head is found close to cyt c_1, as in the native structure, and residues at the docking surface do not undergo any large-scale changes compared to the native structure. Rotations within the pocket lead to an expansion of the proximal domain to accommodate the inhibitor, but the movement of the cd1 helix relative to the -PEWY- loop is less pronounced than that seen with stigmatellin. Although the general orientation of side chains is similar to the native structure, the differences when compared to the stigmatellin structure are quite marked. Rotation of E272 out of the pocket stops it from blocking the proximal domain. Residues lining the ISP access channel move to close the aperture, insulating the Q_o site more from the aqueous phase. This closure involves a rotation of I147 within the pocket and a ~3.5 Å displacement of Y279 to make a H-bond with backbone O of I269. This moves the ef loop and the I269 side chain rotates to close the gap (Figure 5). As noted above, the rotation of E272 out of the pocket is likely to be of functional significance in proton release and may be linked indirectly, through coupled displacements, to the closure of the gap. Compared to the native structure, in which the side chain is also rotated, the displacement of the -PEWY- loop to accommodate the inhibitor brings E272 further from the Q_o binding domain.

Changes similar to those induced by the inhibitors would have to accompany any occupation of the pocket by quinone species. Since only one inhibitor species occupies the volume at a time, the changes associated with their binding may be taken as indicating the accommodations necessary to fit occupants to either the distal or proximal domains.

Mapping the Bifurcated Reaction onto the Bifurcated Structure: Interactions of Quinone with the Reduced ISP, As Detected by Changes in the EPR Spectrum. Some occupants of the Q_o site modify the EPR spectrum of the reduced ISP. Effects of occupancy can be summarized as follows. The inhibitors UHDBT, UHNQ, or stigmatellin induce a new band at $g_x \sim 1.78$ and a shift of the g_y band to lower values (*23*−*26*). In the absence of inhibitors, the spectrum reflects the state of the quinone pool (*31*−*37*). When the Q pool is oxidized, a signal at the $g_x = 1.800$ is observed. When the Q pool is reduced or Q is completely extracted, or with myxothiazole bound at the Q_o site, the g_x line shape changes from a sharp peak at 1.80 to a shallow peak at 1.765. In extraction experiments, Ding et al. (*34*−*36*) observed an intermediate line-shape at 1.783 when ~1 Q/bc_1 complex (in addition to that bound as Q_A) was present. They interpreted the two signals as due to separate species, a tightly binding quinone, Q_{os}, that was bound ~10-fold more tightly than a loosely binding quinone, Q_{ow} (*34*−*36*).

Distribution of Residues at Which Mutation Results in Modified Function: Distinct Domains and Modes of Action. Two binding processes contribute to the catalysis at the site, one involving a binding of the ISP at its docking interface and a second involving binding of quinol in its pocket (Scheme 1). Since the residues contributing to these functions are not a common set, mutations might be expected at the different interfaces, at either of which changes could modify the function of the site. The extensive work from Ding et al. (*34*−*37*) on occupancy of the site in different mutant strains as reflected in the $g_x = 1.80$ signal of the [2Fe-2S] center has contributed a valuable set of data on interactions of the occupant with the ISP. In collaboration with Ding and Dutton, we have made similar measurements on some of our mutant strains from *Rb. sphaeroides* (*43*; B. Barquera, R. Gennis, H. Ding, P. L. Dutton, and A. R. Crofts, unpublished results). The results of these experiments are summarized in Table 1 and Figure 6, which shows residues where change leads to a modified $g_x = 1.80$ signal.

We can distinguish phenotypes for several different classes of mutational change:

(i) Residue Changes Around the Proximal Lobe of the Binding Pocket. Residue changes at M125, Y132, G137, and E272 (yellow) and F129 (orange, in Figure 6), which lead to loss of activity without loss of the $g_x = 1.80$ signal, cluster

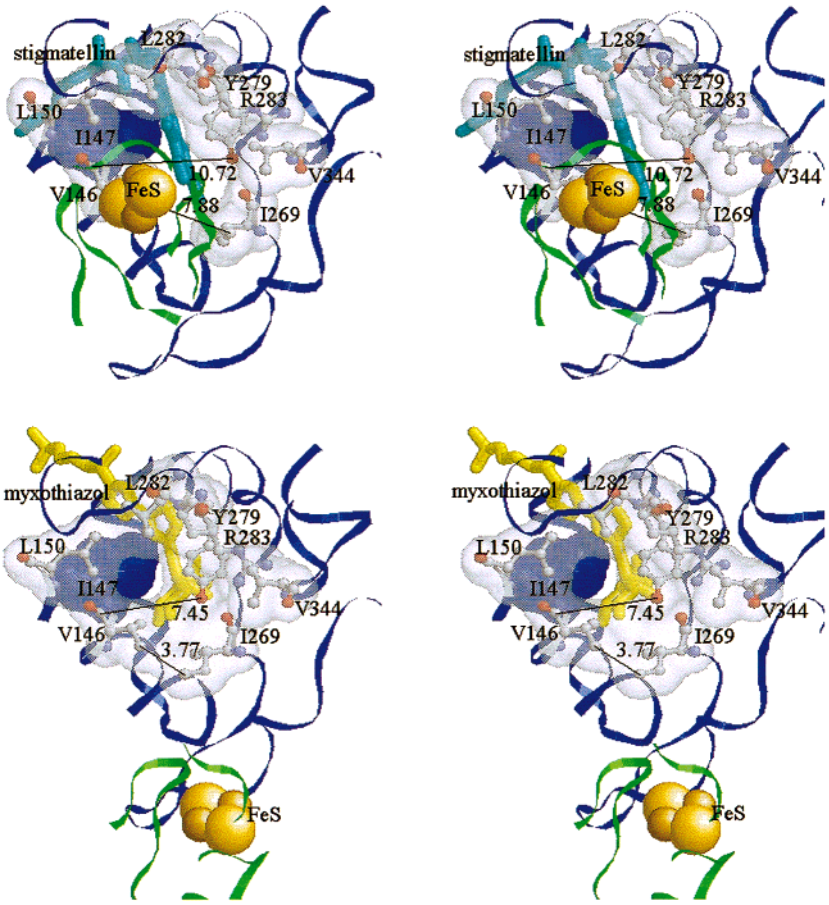

FIGURE 5: Cchange in conformation of the aperture through which the ISP accesses stigmatellin, upon binding of myxothiazole. The residues forming the aperture are shown as ball-and-stick models enclosed by their transparent surfaces. Ile-147 is highlighted as a blue surface. Spans of cyt *b* contributing to the Q_o site are shown by a blue ribbon, and the ISP is shown by a green ribbon, with the cluster as space-filling spheres. The stigmatellin-containing structure is shown with the inhibitor as a cyan tube (top); the myxothiazole-containing structure is shown with the inhibitor as a yellow tube (bottom).

Scheme 1

$$E.c_1^{+}.HISP_C^{red} \leftrightarrows E.c_1 + ISP_C^{ox} + H^{+}$$

$$ISP_C^{ox} \leftrightarrows ISP_B^{ox}$$

$$\begin{array}{ccccc} & & E.b_L.QH_2 & & \\ & \nearrow\swarrow & & \nwarrow\searrow & ISP_B^{ox} \\ QH_2 & & & & \\ E.b_L & & E.b_L.QH_2.ISP_B^{ox} & \leftrightarrows & [E.b_L.QH^{\bullet}.HISP_B^{red}] \leftrightarrows E.b_L^{-} + Q + HISP^{red}(\text{free}) \\ ISP_B^{ox} & \searrow\nwarrow & & \swarrow\nearrow & QH_2 \\ & & E.b_L.ISP^{ox} & & \end{array}$$

at the proximal end of the pocket, closer to the heme of cyt b_L, where the pharmacophore of myxothiazole and MOA-type inhibitors binds. Many of the myxothiazole resistance strains also have residue changes at this end of the pocket (yellow and green in Figure 4), and mutations at all the above residues except E272 show myxothiazole resistance. If the $g_x = 1.80$ signal reflects an interaction between Q and ISP_{red}, then it seems reasonable to conclude that these mutations do *not* interfere with the binding of either of these species. In line with this, for several of these strains (*37*), addition of stigmatellin showed the same EPR line shape change as seen in wild type. However, mutations at these residues do prevent oxidation of QH_2. The structures show that stigmatellin binds at the distal end of the pocket, which suggests that quinone (in the configuration giving rise to the $g_x = 1.80$ signal) also binds there. It seems highly likely that QH_2 (in the configuration in which it undergoes oxidation) binds in this position as well, since all three share the property of interaction with the ISP. In support of this, Ding et al. showed that introduction of a positively charged residue at one of these sites (F144H, -K, and -R, *Rb. capsulatus* numbering, equivalent to F129 in yeast) led to a marked increase in the redox potential of the bound quinone couple, suggesting a tighter binding of the reduced form of the couple, which they explained by formation of an ion pair between the basic residue introduced and an anionic species, suggested to be a ubihydroquinone anion, QH^{-}.

The mutations at E272 (E295D, G-, and -Q in *Rb. sphaeroides*) are particularly interesting from a functional perspective (*43*; Table 1). These all showed an inhibited electron transfer, with maximal rates of 11%, 5%, and <4%, respectively, of that in wild type under the same conditions. However, occupancy of the Q_o site by quinone in the two slowest strains, as indicated by the $g_x = 1.800$ signal, was the same as in wild type. In the stigmatellin structure, E272 forms a H-bond with the inhibitor, and we suggest below that a similar H-bond with the quinol substrate might be formed. From the lack of effect on the $g_x = 1.800$ signal, it seems unlikely that any ligand to the quinone is modified in the mutant strains, suggesting that E272 does not form a ligand to quinone. The loss of a ligand to stigmatellin on mutation of E272 accounts for the otherwise anomalous resistance to this inhibitor, which is in contrast to the

Table 1: Comparison of Q_o Site Occupancy (as Judged by $g_x = 1.80$ Signal) with Activity and Inhibitor Resistance for Cytochrome *b* Mutants[a]

		g_x		activity	resistance or hypersensitivity[b]	
residue	(*Rhodobacter* mutant)	peak location	size	(QH_2 oxidation)	myxothiazole	stigmatellin
M125	(M140R)[c]	1.800	normal	none (ps^-)	I, S	I, (**L**, **N**, **D**)
F129	(F144W, Y)[c]	1.800	normal	normal		
	F144S, V)[c]	1.800	medium	moderate	I, G, L, N	I, G, L
	F144N, I)[c]	1.8−1.78	small	slow	S, A	Y
	F144G, L)[c]	1.78	small	slow		
	(F144H)[c]	1.800	normal	moderate		
	(F144K)[c]	1.791	normal	slow[d]		
	(F144R)[c]	1.818	normal	none[d]		
G131	(G146A, V)[c]	1.77	empty	none (ps^-)		
Y132	(Y147A, S)[c]	1.800	normal	v. slow (ps^-)		
	(Y147F, V)[c]	1.800	normal	moderate		
	(Y147A, S. F. V, stig)[c]	1.786	normal	na		
G137	(G152R)[c]	1.800	normal	fast	T, D, E, H, R, K, C, Y, I, F, L, V, N	
G143	(G158A)[c]	1.800	normal	fast		
	(G158S)	1.800	normal	moderate		
	(G158W)[c]	1.77	small	very slow		
	(G158V, L, I, C, N)[c]	1.765	empty	none		
T145	(T160F)[c]	(empty)		v. slow (ps^-)		
T145	(T160R, S, C, L, Y)[c]	(partially occupied)		slow	(**R, S, C, L, Y**)	
T148	(T163R)[c]	1.765	empty	v. slow	(**V, L, I**)	A, C
P187	(P202L)[e]	1.80	medium	fast		
P187	(P202L, stig)[e]	1.783	medium	na		
N256	(N279Y)[e]	1.80	large	moderate	Y, K, I	Y, K, I
I269	(I292F)[e]	1.78	small	none (ps^-)		
P271	(P294L)[e]	1.77	v. small	none (ps^-)		
P271	(P294L, stig)[e]	1.80	medium	na		
	(P294S)[e]	1.80	large	moderate		
E272	(E295Q)[e]	1.81	large	v. slow		D, Q
	(E295G)[e]	1.80	large	slow		
L282	(L305D)[e]	1.77	small	slow		
	(L305A)[e]			ps^-		
K288	(K329G)[e]	1.77	v. small	moderate		
	(K329A)[e]			ps^-		
G291	(G332S)[e]			moderate		
	(G332I)[e]	1.77	medium	none (ps^-)		
	(G332D)[e]	1.77	small	moderate		

[a] Residue numbers are for chicken (first column) or *Rhodobacter* (second column). [b] Other residue changes at this site giving inhibitor resistance (shown in lightface type) or hypersensitivity (shown in boldface type). Data are from ref 5. [c] Data from refs *5* and *34*−*37*. [d] E_m Q_o/Q_oH_2 raised by binding Q_oH^-. [e] Data from ref *43* and B. Barquera, R. Gennis, H. Ding, P. L. Dutton, and A. R. Crofts.

myxothiazole resistance for mutation to other residues in this set.

(ii) Residue Changes Around the Distal Lobe of the Binding Pocket. Consistent with the model developed above, changes to residues impinging on the stigmatellin binding domain lead to loss of the $g_x = 1.80$ signal (F129, orange; G143, I269, and L282, magenta; and P271, blue, in Figure 6). It seems likely that such mutations interfere with the binding of Q in this domain, and they have variable effects on electron-transfer rate and inhibitor binding. In general, as might be expected, many of the mutational changes giving resistance to stigmatellin are found in this set (red and green residues in Figure 4). Mutations at E272 are an interesting exception; they led to stigmatellin resistance and inhibited electron flow but no loss of $g_x = 1.80$ signal.

(iii) Residue Changes at the Interface with the ISP. Changes at K288, L282, T148, G143, and I269, which can be seen to project into the ISP interfacial surface in Figure 5, eliminate the $g_x = 1.80$ signal (red and magenta in Figure 6). In some cases this was associated with complete loss of activity, but some of these strains showed turnover at an inhibited rate. It seems likely that the mutations in this set interfere with the ISP binding and prevent formation of the complex between Q and ISP^{red} that gives rise to this signal. The variable effects on turnover number would then be explained by the decrease in the residence time of the ISP at the docking interface, and therefore the probability of formation of the reaction complex. We discuss the interface between cyt *b* and the ISP at greater length in a companion paper (*38*).

DISCUSSION

Functional Aspects: Kinetics of the Partial Reactions of Quinol Oxidation. High-Potential Chain and Delivery of Oxidizing Equivalents to the Q_o site. When inhibitors bind at the Q_o site of cyt *b*, they prevent quinol from delivering electrons to the [2Fe-2S] center of the ISP and simplify the electron transfer in the high-potential chain so that the reactions of its components can be examined separately. UHDBT or stigmatellin also prevents the ISP from reacting with cyt c_1 (*23*−*26*). In *Rb. sphaeroides*, oxidizing equivalents from the photochemical reaction center (RC) are delivered to cyt c_1 by cyt c_2, with a $t_{1/2}$ of about 150 μs. The electron transfer from the ISP to cyt c_1, measured in the presence of myxothiazole, cannot be resolved because it is not rate-determining. However, kinetic arguments suggest that the rate constant must be in the range $>10^5$ s^{-1} (*19*, *21*). The reactions of the ISP with its partners (QH_2 bound

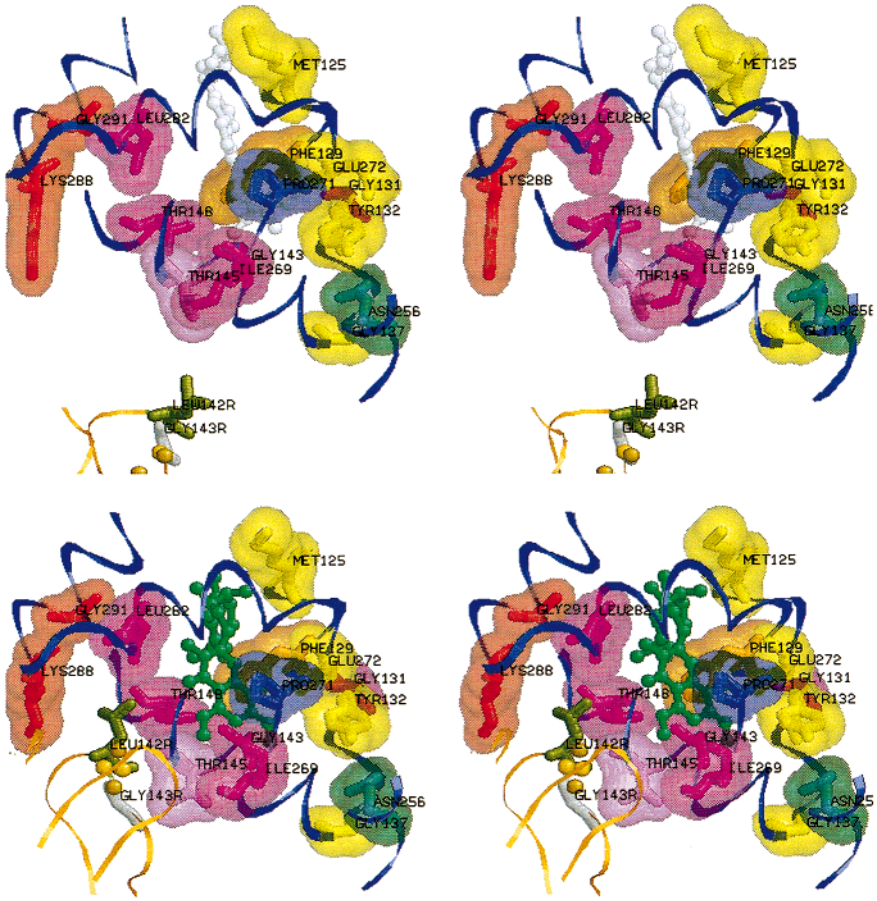

FIGURE 6: Residues at which mutation produces a modified $g_x = 1.80$ band. The view is approximately the same as for Figure 4, but the residues are color-coded according to their effect on the $g_x = 1.80$ signal, as follows: yellow, normal occupancy but no or little turnover (M125, Y132, G137, and E272); red, empty but moderate rate of quinol oxidation (K288, and G291); orange, some mutants are "yellow" and some "red" (F129); magenta, empty and little or no rate (G131, G143, T148, I269, and L282); violet, partially occupied, slow rate, hypersensitive to myxothiazole (T145); blue, P271, where mutant P271L has "magenta" characteristics and mutant P271S has "yellow" characteristics. Residues are shown as tube models, identified by labels at their Cα atoms, enclosed by their transparent surfaces. Inhibitors are shown as ball-and-stick models; stigmatellin (bottom) is green, myxothiazole (top) is white. The iron sulfur protein is shown as a green ribbon, with Leu-142 colored brown and Gly-143 colored gray. Changes at these residues also modify the kinetics of the Q_o site and the $g_x = 1.80$ signal. The [2Fe-2S] cluster is shown by small CPK-colored spheres.

at the Q_o site of cyt *b* and the heme of cyt c_1) require a movement of ~22 Å between two reaction domains on these separate subunits (*7*, *11*, *38*, *39*). In the temperature range < 30 °C, these reactions are rapid compared to the rate-limiting step and do not contribute to the activation barrier for quinol oxidation (*21*, *39*). We have suggested that, apart from binding in reaction complexes, from which it is released by reaction, the forces constraining the ISP head are weak, and the movement is rapid and stochastic (*39*).

Bifurcated Reaction. In the absence of Q_o site inhibitor, and when quinol is available as substrate, the bifurcated reaction occurs, and electrons are delivered to both high- and low-potential chains. Because the reduction of cyt b_H by cyt b_L is not rate-limiting (*16*, *21*), the overall reaction can be assayed by measuring the rate of reduction of cyt b_H in the presence of antimycin to prevent further electron transfer to the Q_i site. In a detailed study of the kinetics as a function of temperature, Crofts and Wang (*21*) developed a model that accounted for the kinetic features of quinol oxidation. For the operation of the Q_o site after delivery of an oxidizing equivalent, the reaction mechanism involved the following steps:

Formation of the Reaction Complex. The reaction kinetics were second-order (first-order with respect to QH_2 in the pool), reflecting binding from the pool and oxidation of QH_2 bound at the Q_o site. The kinetics showed saturation as $[QH_2]$ in the pool increased, typical of a catalytic site, but the maximal rate was reached with the pool still partly oxidized (*15*, *21*, *50*). When the competition between QH_2 and Q for the site was included in a kinetic model (*21*), a higher binding constant for quinol than quinone to the Q_o site (~30−50 times) was needed to account for the saturation.

Oxidation of Bound Quinol; the Activated Step. The estimated rate constant for the oxidation of bound quinol was ~1700 s^{-1} at 25 °C (*21*). The reaction had a relatively high activation energy, which was independent of the degree of reduction of the quinone pool. Because the activation barrier was the same under all conditions of reduction of the pool, Crofts and Wang suggested that the activated step must be after the binding of quinol, in the step leading to formation of the transient semiquinone. The product of probability of occupancy of the site by QH_2 and the forward rate constant determined the overall rate. The activation energy was the same at pH 7.0 and 8.9 for the same initial concentration of substrate, as determined by degree of reduction of the pool (*21*).

Oxidation of Semiquinone, Oxidation of Heme b_L, and Release of product. With both hemes oxidized before flash

activation, no transient reduction of cyt b_L was seen. The reduction of cyt b_L, measured when heme b_H was prereduced, had kinetics similar to those of cyt b_H reduction when both *b* hemes were oxidized before the flash, showing that electron transfer between the hemes was more rapid than the rate-limiting step (*16*). The activation energy was not changed by the reduction of cyt b_H before activation (*21*).

Overall Reaction. In the uninhibited chain, the second turnover of the Q_o site could be followed through the electrogenic processes monitored by the electrochromic carotenoid change. The kinetics showed a monotonic process, indicating that the second turnover followed the first without any lag. This would require release of quinone and binding of quinol, both of which must occur in <500 μs (*15, 18, 19, 51*).

Although the Crofts−Wang model provided an excellent fit to the kinetics over a wide range of conditions, the model needs some refinement in light of the new structural information. In particular, the reaction schemes previously proposed for the Q_o site need to be extended to take account of the movement of the ISP. Since both quinol and the ISP head are mobile species, formation of the enzyme−substrate complex requires docking of both in an appropriate configuration, as summarized in Scheme 1.

In this scheme, cyt *b* with heme b_L is represented by E·b_L, cyt c_1 and its heme are represented by E·c_1, and the docking of the ISP is indicated by subscripts C and B to indicate enzyme−substrate complexes on cyt c_1 and cyt *b*, respectively. The movement of the ISP requires that five catalytic interfaces participate in turnover, rather than the three in current Q-cycle mechanisms.

The modifications above are demanded by the structure. Other aspects of the Crofts−Wang model have been challenged on other grounds: (i) Several different groups (*34−36, 52−54*) have proposed that catalysis involves a synergistic interaction between two quinones occupying the site simultaneously (double-occupancy models). (ii) It has been suggested that the activation barrier involves the binding of quinol (through the need for deprotonation) (*6, 52−54*) rather than events after formation of the enzyme−substrate complex. (iii) It has been suggested that the rate-limiting step is the second electron transfer on oxidation of semiquinone and that the latter is formed as a relatively stable intermediate in the transition complex (*9, 56*).

Several different mechanisms have been proposed to resolve the paradox of the bifurcated reaction (see below), which combine some of the modifications suggested in i−iii above with a variety of switching mechanisms controlled by later redox events (*6, 10, 52−56*).

Paradox of the Bifurcated Reaction. Antimycin, by blocking the Q_i site, acts as an effective inhibitor of net electron transfer by the bc_1 complex. Under steady-state conditions in the presence of antimycin, the low-potential chain becomes reduced, removing heme b_L as an acceptor of the second quinone. The high-potential chain remains oxidized, so that the Q_o site is poised with excess of substrate (quinol and ISP^{ox}) so as to favor formation of the semiquinone product of the first electron-transfer reaction. The behavior under these conditions is referred to as oxidant-induced reduction. Crofts and Wang (*21*) could detect no myxothiazole sensitive semiquinone under these conditions and therefore concluded that the equilibrium constant for formation of semiquinone was very small and that $\Delta G°'$ was large and positive and might contribute a significant part of the activation barrier. This view has recently been reinforced by similar observations in mitochondrial preparations (*22*). In the presence of O_2, an antimycin-insensitive electron transfer is observed, and this has been attributed to reduction of O_2 to O_2^- by semiquinone (recently reviewed in ref *57*). Similarly, under anaerobic static-head conditions, electrons accumulate on heme b_L, due to back-pressure from the proton gradient, but flux is minimal and mainly attributable to proton leakage or O_2^- formation rather than mechanistic decoupling (*57, 58*). It is clear from the low leakage rate that if any semiquinone is formed, it is unable to reduce the high-potential chain directly. Several different explanations have been proposed to account for this paradoxical behavior, which need to be reevaluated in the new structural context.

Functional Role of the Proximal Lobe. The functional significance attributed to the bifurcated volume of the Q_o site depends heavily on interpretation of the $g_x = 1.80$ signal and the various effects leading to its modification. The following explanations for this signal have previously been suggested:

(i) Double-Occupancy Models. Ding et al. (*34−36*) interpreted changes in the g_x signal in the context of their double-occupancy model. They suggested that the species interacting with the ISP to transfer the first electron would likely be the strongly binding component, Q_{os}. In the context of the structure, this would have to occupy the distal domain. Because of the apparently weak binding, Ding et al. suggested that Q_{ow} would be the exchangeable species through which coupling to the quinone pool could occur. The signature of the weakly binding species, the EPR band at $g_x = 1.80$, was therefore ascribed to Q_{ow}. Brandt et al. (*30*) had previously interpreted kinetic experiments with MOA-type inhibitors as indicating that quinol and inhibitors could bind independently at the Q_o site and have more recently suggested that this provides support for double-occupancy models (*6, 52−54*). On the basis of this interpretation, Brandt and colleagues (*6, 52−54*) have extended their "catalytic switch" model to suggested a proton-gated charge-transfer mechanism, including sym proportionation within a quinhydrone-like structure at the Q_o site.

(ii) Single-Occupancy Models. In the Crofts and Wang model (*21*), the Q_o site reaction proceeded via a single bound QH_2, which competed with Q for occupancy. From an analysis of the structure, Crofts et al. (*40*) suggested that the $g_x = 1.80$ signal was due to the reduced ISP docked at the interface on cyt *b* (ISP_B configuration), interacting directly with quinone in the distal domain of the Q_o site, and that the signal is lost whenever this complex cannot form. They suggested that all interactions of the Q_o-site occupant with the ISP must be from this distal position and that the reactions involved a single occupant.

(iii) Functional Dimer. De Vries et al. (*32, 33*) had earlier proposed that the bc_1 complex operates through a functionally dimeric structure. They suggested that the different EPR signals were associated with different states of the ISP in the two monomers of the dimeric complex and that turnover required exchange of redox equivalents between monomers. Gopta et al. (*55*) have recently suggested a dimeric function from kinetic experiments in *Rb. sphaeroides*.

The structures provide a basis for deciding between double- and single-occupancy models. Although it has been claimed that the bifurcated volume of the Q_o site provides a structural justification for double occupancy (*6*), the following points do not support double occupancy:

(1) None of the structures shows any well-resolved density in the uninhibited site. At the least, a tightly bound Q_{os} species would be expected in the Ding and Dutton model (*34*, *35*). From the relatively low quinone content of the crystals (<1 Q/cyt c_1), and the occupancy of the Q_i site by a well-defined quinone (~0.79 in both monomers, calculated from electron densities), we can conclude that, in our native crystals, the binding at the Q_i site is stronger than at the Q_o site and that the quinone content is accounted for by the Q_i site occupant (*7*). In the structure of Xia et al. (*8*), the authors reported no loss of density from the Q_o pocket upon binding of Q_o-site inhibitors, although a loss of density was observed at the Q_i site upon binding of antimycin, and this was attributed to displacement of quinone. Since their crystals also contained substoichiometric levels of quinone (~0.75 Q/complex), these results would also suggest that the Q_i site binds the quinone more tightly than the Q_o site.

(2) In our structures, all the Q_o site inhibitors occupy overlapping volumes (see Figures 2 and 4). The tunnel through which the tails access the lipid phase has a cross-sectional area not much greater than that of a tail. Occupancy would be constrained in the tunnel, and the adjacent volume of the pocket, to one entity. Compared to the native structure, occupancy by either class of inhibitor led to an expansion of the pocket. If a disordered quinone occupied the pocket in the native structure in either domain, inhibitor binding would lead to displacement, and expansion would not have been expected. Occupancy by two quinones would require a major expansion of the protein to widen the tunnel and the adjacent volume. From the substantial expansion of the site on binding inhibitor, it seems unlikely that any quinone species of similar volume (much less two) was displaced.

The structures are in good agreement with inhibitor competition studies (*23*−*29*), which have shown that tailed Q_o site inhibitors are mutually exclusive occupants. Ding et al. (*34*) showed that tight-binding inhibitors of either class could eliminate the EPR signals attributed to both Q_{os} and Q_{ow} at concentrations stoichiometric with the complex, presumably by displacing the occupant. These results suggest that only one tailed inhibitor species can occupy this volume (but see ref *10*) and that occupation by inhibitor displaces all ubiquinone 10.

(3) Brandt et al. (*30*) interpreted inhibitor titrations of steady-state turnover as showing a noncompetitive inhibition of quinol oxidation by MOA-type inhibitors. From this work, and binding studies, they concluded that inhibitor and substrate could bind simultaneously at the Q_o site. This conclusion seems in contradiction with the structure, with the extensive literature on competition between different classes of inhibitor (*23*−*29*), and with the effect of inhibitors on the g_x signals shown by Ding et al. (*34*). In interpreting their kinetic data, Brandt et al. (*30*) used a classical noncompetitive scheme in which the inhibitor could bind to both enzyme ($E + I \leftrightarrows EI$) and enzyme−substrate complex ($ES + I \leftrightarrows ESI$). Such a scheme is only appropriate under conditions in which all equilibria determining the concentration of ES are rapid compared with the dissociation of ES to product (P). This would be the case only with a weakly binding inhibitor, with on and off rates rapid compared to turnover. Inhibitor titrations of the single turnover of the Q_o site assayed by flash activation of *Rb. sphaeroides* chromatophores show unambiguously that myxothiazole and MOA-type inhibitors bind tightly from the membrane phase. Dissociation of the inhibitors was several orders of magnitude slower than the turnover time of the reaction (A. R. Crofts, M. Guergova-Kuras, S. Hong, unpublished results). The use of such a scheme was therefore inappropriate, and the conclusions derived by Brandt et al. (*30*) were not justified. The inhibitors show noncompetitive effects because they remove enzyme from the reaction mixture by binding tightly to E, not because they bind to ES.

(4) From the double-occupancy mechanism of Ding et al. (*34*−*36*), it might be expected that the catalytic site would contain two distinct sets of ligands to provide for the differential binding of the two species. From the structure, the two quinones would have to occupy the two domains. Although numerous single-site mutations that differentially affect binding of stigmatellin or myxothiazole (or inhibitors of equivalent class) have been characterized, no similar differential effects on Q_{ow} and Q_{os} have been observed (*34*−*37*, *40*, *43*).

(5) The EPR spectrum of the [2Fe-2S] center in the isolated ISP fragment (*59*) has g_x, g_y, and g_z values similar to those in the complex in the presence of myxothiazole, consistent with the fact that myxothiazole and MOA-type inhibitors do not modify the spectral or redox properties of the ISP, and did not displace the ISP from the position in our native structure. These factors suggest that the ISP does not interact with any Q_o-site occupant in the presence of these inhibitors. By extension, the $g_x = 1.80$ signal is due to some liganding function specific to the quinone-occupied complex. It seems likely that this function is a direct interaction between the quinone at the Q_o site and the reduced ISP at the docking interface on cyt *b* (*40*) and that the contacts seen between stigmatellin and the ISP in the stigmatellin cocrystals demonstrate the spatial location of this interaction. This conclusion is well supported by the effects of mutation noted above.

(6) The remaining evidence for double occupancy comes from interpretation of the change in g_x line shape when quinone is extracted from chromatophores (*34*, *35*). Paradoxically, as noted above, other properties attributed to the Q_{os} and Q_{ow} species were similar. This paradox could be resolved if the line shape change reflected only one species. However, this would require a different interpretation of the $g_x = 1.783$ signal. We do not claim to explain this signal, but we note several possibilities:

(i) Interpretation of $g_x = 1.783$ in terms of a tight-binding species ignores complications arising from the heterogeneity in distribution of redox components. Statistical effects on distribution at random will ensure that the components are not evenly partitioned into reaction domains (cf. ref *60*). If each component partitioned separately, the range of stoichiometric ratios in individual domains would vary widely from the mean ratio (normally ~ 2:1:1 for RC:bc_1:cyt c_2), especially in a partitioned system like chromatophore vesicles. Extraction, or reconstitution of fully extracted chromatophores, to the point giving rise to the Q_{os} signal would also leave a random distribution of quinone. Even if

a tight-binding Q_{os} species were present, in the chromatophores with an excess of Q, one would expect to see a sharp peak at 1.80 due to Q_{ow}, while in another fraction, the quinone would be low, leaving some bc_1 complex without a quinone, with a shallow peak at 1.765. This mixture of populations would give in the overall population a peak representing the convolution of these two spectra, at a position intermediate between them. A fraction of the $g_x = 1.783$ peak could be attributed to such a mix.

(ii) Because of the kinetic importance of the reaction complex between ISP and quinol, it seems quite possible that some preferential local binding that would favor a local concentration of the ISP head might occur and increase the probability of formation of the complex (*47*). It is possible that the $g_x = 1.783$ peak reflects a preferential occupancy of such a standby position on extraction of quinone.

(iii) If the ISP is mobile, the environment of the [2Fe-2S] center (including interaction between the spins of the reduced [2Fe-2S] center and the oxidized cyt b_L; *24*), and the protein interactions of the ISP, will reflect a heterogeneity of binding domains. Any change in occupancy of the Q_o site might lead to redistribution. Some perturbation of the spectrum of the [2Fe-2S] center might be attributed to these changes.

In view of these difficulties, we believe that, before a compelling case can be made for double occupancy, more direct evidence is needed to show that the $g_x = 1.783$ band is due to a quinone tightly bound as a separate species at the Q_o site. The anomalous factors outlined above can be explained in the double-occupancy model only through ad hoc hypotheses. The changes of the $g_x = 1.80$ signal have a simple interpretation, in line with a single occupancy: (a) The $g_x = 1.80$ signal is associated with a complex formed between quinone bound in the Q_o site at the distal end and the reduced ISP docked firmly at the interface with cytochrome *b*. (b) The signal is lost whenever this complex cannot form. (c) Only one quinone species occupies the site.

With respect to the functional dimer model, the structures show that both pairs of quinone processing sites are widely separated in the dimeric structure (~35 Å for Q_i sites, ~49 Å for Q_o sites) and connected only through their access to the common lipid or aqueous phases. Although, as pointed out by Xia et al. (*8*), the cyt b_L hemes are quite close together (~21 Å between parallel hemes), there is no indication from kinetics studies or inhibitor binding that rapid redox exchange occurs between monomers in the complex (*23*). These structural features make it unlikely that cooperation between sites can be important to function as suggested in the mechanism of De Vries et al. mechanism (*32*, *33*; see also ref *55*).

Bifurcated Reaction: Possible Factors That Might Prevent Reaction of the Semiquinone with ISP^{ox}. Several different mechanisms have been proposed to resolve the paradox of the bifurcated reaction. (1) The properties of the reaction complex at the Q_o site, formed as a prelude to the oxidation reaction, might determine the fate of the reaction products. In the model proposed by Crofts and Wang (*21*), the reaction complex would persist until dissociation to products on transfer of the first electron. The high activation energy, and the fact that the semiquinone product was not detectable, provided possible constraints on the equilibrium constant. Rapid removal of products would ensure an efficient bifurcation in the normal forward electron transfer. Jünemann et al. (*22*) have recently argued the same case in the context of the mitochondrial complex. The structures provide an additional perspective; because of the large distance between its two reaction interfaces, the reduced ISP would be insulated from its acceptor until liberated by dissociation of the reaction complex. If the probability of dissociation were low enough, this would ensure that the dissipative reaction would be slow and the bifurcation therefore efficient. However, this explanation requires that the pathway for transfer of the second electron to heme b_L should have a very high intrinsic rate constant compared to the pathway to ISP^{ox}.

(2) The efficiency of the bifurcation (or the failure of the semiquinone to reduce the oxidized [2Fe-2S] center) could possibly be explained if the displacement of the ISP subunit removed it from the interface with the Q_o site. It would then no longer be available to act as an oxidant for the semiquinone. However, this explanation seems simplistic, since in the oxidized state the ISP would have to detach easily from its association with cyt c_1, and the structures show that association constants for the oxidized ISP at both docking interfaces are small (*39*). Since the diffusion time is short, we might expect the oxidized ISP to be readily available to the Q_o site, regardless of occupancy, unless some specific change at one or other of the catalytic interfaces hindered access.

(3) Following an idea of Lancaster and Michel (*61*) based on work with reaction center structures with stigmatellin in the Q_B site, Link (*56*) suggested an alternative role for the reaction complex. If electron transfer could occur within the reaction complex without dissociation, the resulting intermediate state would include a ligand between the semiquinone and the reduced ISP. Link (*56*) suggested that ligation would change the redox properties of both species, as seen in the inhibitor−ISP^{red} complexes (*23*−*26*). If the E_m of the ISP were raised enough, this would constrain the ISP from reaction with cyt c_1 until the semiquinone was oxidized:

$$QH_2 + ISP^{ox} + b_L^{+} \rightarrow [QH^{\bullet}-ISP^{red}\cdot b_L^{+}] \rightarrow \{Q-ISP^{red}\cdot b_L\}^n \rightarrow Q + ISP^{red} + b_L + 2H^{+} \quad (1)$$

In the context of an electron-transfer chain with fixed redox centers, these two features of the reaction complex provided an attractive explanation for the paradox of the bifurcated reaction. However, a significant difference between this scheme and that of Crofts and Wang lies in the electron-transfer process associated with the transition state. In the Link model, the transfer of the second electron represents the limiting step.

(4) Kim et al. (*10*) have favored a model in which "the two electrons of ubiquinol in the complex are transferred simultaneously, one to FeS, and the second to heme b_L", but they did not suggest a mechanism by which this could happen.

(5) Brandt and von Jagow (*62*) proposed a "catalytic switch" model, in which they suggested that redox-linked conformational changes might prevent the occupant of the quinone binding pocket from reacting with the ISP at critical points in the reaction cycle. This general idea is in line with the movement of the ISP seen in the structures (*7*) and the

changes in conformation on binding inhibitors. Since similar changes likely accompanying changes in occupancy by catalytic intermediates, these might provide a mechanism for such a switch. Iwata et al. (*9*) have extended this idea in the context of the intermediate (int) position found for the ISP head in one monomer of the $P6_5$ crystal form. They have suggested a catalytic cycle with three states and switching determined by redox events in the *b*-cytochrome chain. Kim et al. (*10*) have suggested that a switch from a cyt *b* bound to a free state is linked to electron transfer between hemes b_L and b_H.

(6) Displacement of the semiquinone to a position deeper in the pocket and closer to its reaction partner, the cyt b_L heme, so as to remove it from the reaction interface seen by ISP^{ox} would also discourage the dissipative reaction. We have suggested this as a modification of the Crofts−Wang model (*7*, *11*, *40*).

The possibilities numbered above are not all mutually exclusive. The properties of the reaction complex formed at the Q_o site are likely to be critical. Earlier work from this lab had shown that the rate of quinol oxidation is determined by the probability of quinol binding, as shown by the second-order nature of the reaction (*15*, *21*, *50*). We have more recently shown evidence that the oxidized ISP in its dissociated form reacts to form the complex and that the pH dependence of the rate in the acidic range reflects the availability of this species (*41*, *42*, *49*). Neither binding process contributes to the activation barrier, which is in the reactions after formation of the complex. We had previously observed that the activation barrier was the same at pH 7.0 and 8.9 (*21*) and have reported preliminary experiments to extend this range down to pH 5.5 (*42*). The lack of any pH dependence over this range would exclude dissociation of QH_2 to QH^- as the event determining the activation barrier. A full discussion of these results, and the contrasting data of Brandt and Okun (*6*, *52*−*54*), will be provided in a separate paper (*67*).

We have argued above that the structural information makes it unlikely that the site functions through double occupancy, and our kinetic data show that the activated step is after formation of the enzyme−substrate complex, not on dissociation of QH_2. The remaining reaction pathways that seem plausible are single-occupancy models. In the model of Link (*56*), the electron distribution between the quinol and the ISP favors formation of semiquinone in the reaction complex, and dissociation of the complex occurs after transfer of the second electron. In the model of Kim et al. (*10*), electron transfer occurs from the reaction complex at the distal domain, and the suggestion of a simultaneous electron transfer implies that the concentration of intermediate is vanishingly low. In the modified Crofts−Wang model, dissociation of the complex occurs on the first electron transfer to form semiquinone (which remains in the Q_o site) and ISP^{red} (available for diffusion to cyt c_1). In all mechanisms, the reaction complex is a single species, and the activation barrier is in the reaction leading to dissociation of the transition state. The Link model would clearly be more attractive if additional evidence was available to demonstrate the expected semiquinone and reduced [2Fe-2S] at the Q_o site. As Jünemann et al. (*22*) have pointed out, the failure to detect any semiquinone at the site does not necessarily exclude the Link mechanism, because interactions between spins might make both invisible to EPR. Other spectroscopic methods might be used to test this hypothesis. In addition, as noted by Brandt (*53*), the oxidant-induced reduction conditions may bias the reaction against semiquinone production. This would be the case if a semiquinone anion was the product and the charge on ferroheme b_L exerted a local Coulombic effect.

For the models discussed above, the forward reaction proceeds from a reaction complex between quinol in the distal lobe, and oxidized ISP at the docking interface on cyt *b*. We favor a model in which electron transfer to form the semiquinone weakens the bond between His-161 and the occupant, and bond breakage leads to dissociation of the reaction complex to form a bound semiquinone species unliganded by the free ISP^{red}, which is the other product. We suggest that this is the activated step. We argue below that further advancement of the reaction would involve a displacement of the semiquinone from the site of its formation in the distal lobe to the proximal lobe, closer to heme b_L. This movement is represented in eq 2 by the subscripts to Q indicating distal (d) or proximal (p) domain occupancy:

$$QH_2 + Fe_2S_2^{ox} + b_L \rightarrow [Q_dH_2{-}Fe_2S_2^{ox}{\cdot}b_L \leftrightarrow Q_dH^{\bullet}{-}HFe_2S_2^{red}{\cdot}b_L] \xrightarrow{K} Q_pH^{\bullet}{\cdot}b_L + HFe_2S_2^{red} \quad (2)$$

where $2 \times 10^{-4} > K > 2 \times 10^{-8}$. Several lines of evidence suggest that the equilibrium constant for the first electron transfer is very small and that the semiquinone is unstable (*21*). In the coupled steady state, heme b_L and cyt c_1 are poised near their midpoints (*58*), so a relatively unstable semiquinone would be necessary to generate a reductant of sufficient power to donate to cyt b_L and drive electrons across the membrane against the proton gradient. The production of O_2^- is further evidence that a strong reductant is generated at the site (*57*). For the reaction of eq 2, Crofts and Wang (*21*) estimated a maximal value of $<2 \times 10^{-4}$ for the overall equilibrium constant, based on their inability to detect in *Rb. sphaeroides* any significant semiquinone under conditions of oxidant-induced reduction that would be expected to maximize the concentration by mass-action effects. Jünemann et al. (*22*) have obtained the same result with mitochondrial preparations; they showed that the semiquinone previously attributed to the Q_o site by De Vries et al. (*33*) was not seen when specific Q_o-site inhibitors were present. The maximal value discussed by Crofts and Wang was based on an estimate of the signal-to-noise ratio of the EPR measurements (*64*; K. Andrews, A. R. Crofts, and R. Gennis, unpublished results); the Jünemann et al. (*22*) data show a somewhat better signal-to-noise ratio, so this value could now be set lower. A minimal value ($K > 2 \times 10^{-8}$) is provided by the ∼45 kJ/mol activation energy (*21*, *39*).

Role of the Proximal Domain. None of the reaction complexes discussed above have properties that account for the critical importance of residues in the proximal domain of the Q_o site. Since quinone can bind in mutant strains with an inhibited electron transfer, it seems likely that the substrate can also bind at the site and form a reaction complex with ISP^{ox} (see above). The inhibition of oxidation in these mutants must therefore reflect some other effect relating to

occupancy of the proximal end of the pocket, or to function. For M125, Y132, G137, and F129, the effects of mutation to introduce myxothiazole resistance clearly point to an effect on occupancy of the inhibitor and suggest that the inhibitory effect on electron transfer might also reflect a constraint on occupancy by a reaction intermediate. For E272, both these roles are indicated. Rotation to the out positions removes a physical blockage of the proximal domain, and a functional role in proton release seems likely (*49*).

In the absence of evidence for a firmly bound quinone in the site, the inhibition of electron transfer by mutations in the proximal domain could most readily be explained by a need for movement of the semiquinone into this domain to bring it closer to cyt b_L to allow rapid electron transfer. Because the reaction complex forms with quinol in the distal domain, the reactants are rather distant from the heme b_L, which acts as an acceptor for the second electron. Movement of the semiquinone to the proximal position would decrease the reaction distance (from ~11 to 5.5 Å) and increase the reaction rate for reduction of heme b_L. It would also increase the distance between the semiquinone and the [2Fe-2S] center in the ISP_B configuration and thus eliminate any possible through-ligand electron-transfer pathway to the ISP^{ox}. This kinetic impediment would be enhanced if conformational changes similar to those seen on binding myxothiazole or MOA-stilbene helped to insulate the pocket (Figure 5). This insulation would also protect against reduction of O_2 to superoxide. Such protection would likely have been an important development in the early evolution of the complex, which allowed safe operation of the bifurcated reaction at ambient $[O_2]$. The possibility of such a movement is supported by the deeper position in the pocket of myxothiazole compared to stigmatellin (cf. Figures 3, 4, and 6), and by the occurrence of similar changes in photochemical reaction centers. Stowell et al. (*63*) have shown a substantial movement of Q_B when it is reduced in its binding pocket, including a displacement of 4.5 Å from a distal to a proximal location, and a twist of 180° around the tail. The movement at the Q_B site would have to occur within the measured reaction time of ~30 μs, so a similar kinetics for movement at the Q_o site could be much faster than the rate-limiting step. Alternative positions for quinone binding in the Q_B pocket are also apparent from the work of Lancaster and Michel (*61*).

Structural and Theoretical Constraints on the Rate Constants. We have noted above a critical difference between the modified Crofts-Wang mechanism and the Link (*56*) mechanism. The step with a high activation barrier occurs on the first electron transfer in the former and on the second electron transfer in the latter. Constrains on rate constant determined by distance in the structures, and the high activation barrier, limit the choice of mechanism, as discussed below.

For the models of Link (*56*) and Kim et al. (*10*), the second electron transfer to heme b_L has to occur from semiquinone in the complex with ISP. Because the reaction complex involves a tight liganding to the ISP, it must be formed at the distal end of the pocket. From the structures we can estimate maximal rate constants for the electron transfer from semiquinone to heme b_L, using the crystallographic distances (*7*). For $R = 11$ Å, the distance between stigmatellin and the heme edge, appropriate for semiquinone in the distal domain, $k_{max} = 2.51 \times 10^8$ s^{-1} when $-\Delta G = \lambda$ (*65*). However, this presupposes that an appropriate through-bond pathway to span this distance would be available; the structure shows that the intervening protein is from helix C, perpendicular to the path, and with no contacts to the distal domain occupant, so this k_{max} value is likely too high. The true rate constant will depend on the matching between $-\Delta G$ and λ, both of which are related to the activation energy through the Marcus equation, $\Delta G^{\#} = (\lambda + \Delta G^{\circ\prime})^2/4\lambda$ (see ref *66*). Since $\Delta G^{\circ\prime}$ for reduction of heme b_L is close to 0 (*15*, *21*), $\lambda \approx 4\Delta G^{\#}$, giving a value of ~2 eV for an activation energy of 45−50 kJ·mol^{-1}. Applying these values to the equation given by Moser et al. (Dutton's ruler, *65*), we obtain a rate constant of 158 s^{-1}. The product of the rate constant and the concentration of the semiquinone substrate would determine the rate of the reaction, but estimations of these values are not independent. There is an interesting tradeoff between rate constant and semiquinone concentration that depends on the contribution of semiquinone stability to both occupancy and ΔG for the second electron transfer. For the distance of 11 Å from a distal domain occupant, a value for λ of 2 eV (higher values would give lower rates), and published values for E_m of the redox centers, no obvious combination of reaction parameters would provide a rate for reduction of heme b_L as fast as that measured. If the occupancy was determined by the activation barrier ($[QH^{\bullet} - ISP^{red}] \sim 2 \times 10^{-8}$), as seems to be implicit in the mechanism Kim et al. (*10*), the maximal rate would be < 1 s^{-1} (depending on choice of λ), 3 orders of magnitude less than needed. The Marcus relationship would limit mechanisms to those in which electron transfer from the distal domain occurred after the activation barrier, allowing only those models in which the activation barrier is in the first electron-transfer reaction (*21*).

For the modified Crofts−Wang mechanism, the first electron transfer would be through the bridging His-161 and the intrinsic rate constant would be very high and would not provide a kinetic constraint, even with a high value for λ. However, the expected concentration of semiquinone product could be very low (*21*), and the rate constant from the distal domain could then be limiting. Since the second electron transfer would be after the activation barrier, the value for λ would certainly be lower than for the first electron transfer. For electron transfer from the proximal domain, the rate constant would be at least 3 orders of magnitude higher than from the distal domain. The distance between myxothiazole and the heme edge ($R = 5.5$ Å) is appropriate for electron transfer from semiquinone in the proximal domain, giving $k_{max} = 5.01 \times 10^{11}$ s^{-1} when $-\Delta G = \lambda$. The intervening protein contacts both occupant and heme b_L and so provides several possible pathways. Even if the activation energy determined the concentration of semiquinone, a rate of $(1-3) \times 10^3$ s^{-1} (depending on choice of λ) would be expected, compatible with the measured rate. Contrary to the suggestions of Jünemann et al. (*22*) and Kim et al. (*10*), the failure to detect a semiquinone at the Q_o site does not preclude a movement from distal to proximal domains. Indeed, the constraints of distance, redox poise, activation barrier, and λ map out a limited set of options for models; if the time-averaged concentration of semiquinone is in the range suggested by experiment (see above and refs *21*, *22*, *39*, and *42*) and λ is greater than 1, the measured rate would

require movement to the proximal domain. We discuss the energy landscape of the reaction at the Q_o site in greater detail in the context of measurements of the activation energies for the partial reactions over the pH range 5.5−8.9 (*39*, *42*, *67*).

The slowed electron flow in mutants with residue changes in the proximal pocket (see above) is of interest in this context. As discussed above, we would anticipate that, in these strains, the reaction complex of eq 6 would still form at the distal lobe. We have suggested that these strains were inhibited by a constraint that prevented occupancy of the proximal lobe. If electron transfer normally occurred from the distal configuration (*10, 56*), an alternative explanation for the inhibition will be required. If the reaction complex could dissociate with high probability so as to liberate ISP^{red}, we would expect to see a rereduction of cyt c_2 and c_1 decoupled from the bifurcated reaction. The kinetics therefore provide a test of the stability of the complex. In our experiments, these strains show a strongly inhibited electron transfer to the high-potential chain, suggesting that, if it forms, the reaction complex does not readily dissociate (B. Barquera, and A. R. Crofts, unpublished results).

CONCLUSIONS

In summary, we suggest the following overall mechanism for turnover of the Q_o site of the complex, as illustrated in Figure 7:

(a) Oxidizing equivalents are transferred to the site through cyt c_1 and the ISP. The mechanism involves a movement of the ISP between reaction domains on cyt c_1 and cyt *b*, as suggested previously (*7*) and discussed at length in separate papers (*38*−*40*).

(b) The reaction proceeds from an enzyme−substrate complex between the oxidized ISP and quinol at the Q_o site. Formation of the complex involves binding of QH_2 at the distal end of the Q_o pocket and binding of the oxidized ISP, in its dissociated form, at the interface on cyt *b* (Figure 7A). The site changes conformation to accommodate the substrates. The stigmatellin structure suggests that the complex involves hydrogen bonding from His-161 of the ISP (*7*) and Glu-272 of cyt *b*. The ISP acts as a H-carrier, to remove the electron and the first proton on oxidation of QH_2 to semiquinone (*41, 42*) (Figure 7B,C). The H^+ is released on oxidation of the ISP, either immediately (at pH above the p*K* of ∼7.6 on the oxidized form) or before formation of the next reaction complex (at pH below the p*K*).

(c) Electron transfer from QH_2 to the ISP leading to formation of semiquinone is the reaction with a high activation barrier (*21*). Since the equilibrium constant for formation of semiquinone is too small to measure, formation of the semiquinone is improbable, the reaction complex between quinol and ISP^{ox} is relatively long-lived, and the positive $\Delta G°$ for formation of semiquinone likely contributes to the high activation barrier. The semiquinone is a transient species because, once formed, it is removed rapidly. Because the subsequent reactions of both high- and low-potential chains are not rate-determining, electrons appear at the acceptor termini (cyt *c* for the high-potential chain and cyt b_H for the low-potential chain blocked by antimycin) with the same kinetics, determined by the rate-limiting step.

(d) We suggest that, as a necessary step, the semiquinone moves in the pocket to the proximal end, near heme b_L, which facilitates its rapid oxidation (Figure 7C,D). This movement also requires changes in the protein conformation, which may contribute to the activation barrier. Although in normal turnover the semiquinone is rapidly oxidized, under static head conditions, since cyt b_L is poised half-reduced, a kinetically significant (but not necessarily detectable) population of semiquinone might be expected at the site. The movement of semiquinone to the proximal domain and closure of the aperture (Figure 5) would insulate it from further reaction with the reoxidized ISP, or with O_2, and thus minimize the decoupling of electron transfer from proton pumping or formation of superoxide anion.

(e) The semiquinone passes its electron to the cyt b_L heme, and thence to heme b_H, and the quinone exits the Q_o site. In the absence of antimycin, the electron is transferred to the Q_i-site occupant.

(f) At some point between steps c and e, the second proton is released. The structures suggest that this occurs through protonation of Glu-272 and rotation of the side chain, followed by dissociation and exit of the H^+ via the water chain proposed in ref *47* and discussed above (Figure 7B,C) (*49*). Since rotation of Glu-272 away from the pocket is required to allow movement to the proximal domain, this would suggest that deprotonation of the semiquinone occurs before oxidation (after step c and before step d above), so that the semiquinone anion moves and donates to heme b_L (steps d and e).

(g) Meanwhile, the reduced ISP can deliver an electron to cyt c_1 by tethered diffusion (*38, 39*) and return in the oxidized form to initiate another turnover of the Q_o site.

This mechanism is compatible with all the structural and kinetic data presently available, and it explains the efficiency of the bifurcation process with satisfactory parsimony. However, we recognize that other mechanisms are possible. As discussed at length above, we believe that double-occupancy models are unlikely. Double occupancy would require a very substantial expansion of the Q_o site, especially the tunnel to the lipid phase, and none of the structures, or the prior competition experiments, suggest that this could happen with high probability. However, we cannot rule out such a possibility. If future work shows that two quinones can occupy the Q_o site, some modification of the model of Ding et al. (*34, 35*) would be needed. From the structure, it is clear that all interactions with the ISP must occur from the distal domain, and the pattern of mutational change suggests that the $g_x = 1.800$ signal reflects an interaction of Q in this domain with ISP^{red}. Since the signal is diagnostic, Q_{ow} would have to occupy this distal site and Q_{os} the proximal site, with the latter as a more permanently bound species acting as an electron shuttle to heme b_L on formation of the semiquinone on the former. Among single-occupancy models, we favor that outlined above, since it provides an explanation for the importance of the proximal domain and a mechanism for protection against O_2^- production. However, we cannot rule out models in which electron transfer occurs to heme b_L from the distal domain. For such models, the constraints of energy barrier and distance on rate constant rule out electron transfer from a semiquinone in the distal domain that involves the activation barrier.

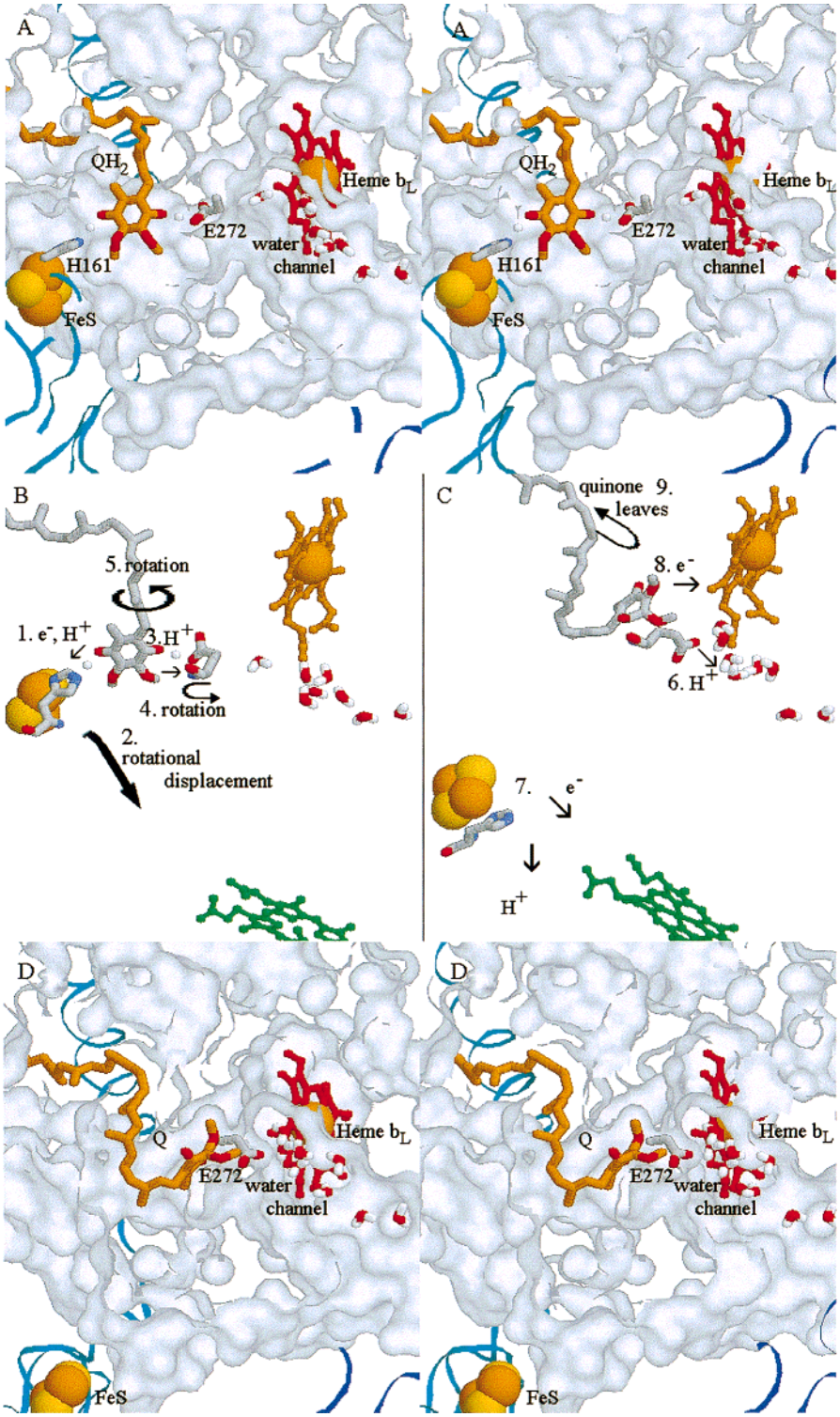

FIGURE 7: Mechanism of the bifurcated reaction. Cyt *b* is shown by the protein surface, and the other catalytic subunits are shown as ribbons (ISP is light blue, cyt c_1 is dark blue), with prosthetic groups shown as ball-and-stick models, except for the [2Fe-2S] cluster, which is shown as spacefilling spheres. The cyt b_L heme is colored red (A, D) or orange (B, C), and heme c_1 is green-blue (B, C). Quinone species at the Q_o site were modeled in structures with the inhibitor removed, as follows. For panels A and B, the stigmatellin-binding structure was used. For panels C and D, the myxothiazole-binding structure was used. The quinone was positioned as detailed in the Materials and Methods section. (A) Reaction complex between QH_2 bound in the distal domain (C atoms in orange in panel A, gray in panel B), and ISP^{ox} bound at the interface on cyt *b*. Note Glu-272 shown in the position in the stigmatellin-containing structure, which also provides a H-bond to quinol. The water molecules in the water channel are abstracted from the model constructed for a steered molecular dynamics simulation of the ISP movement (*47*). (B, C) Reactants in the positions for the enzyme−substrate complex (left) or the enzyme−products complex (right), with the separate processes contributing partial reactions discussed in the text. The numbers show a possible sequence of reactions. (D) The reaction complex has dissociated to products, and the ISP^{red} has moved to the position close to cyt c_1. The quinone (or semiquinone anion, gray in panel C, orange in panel D) has flipped to the proximal domain. Note the position of Glu-272, now rotated out of the pocket, and connecting to a channel into cyt *b* from the P-side aqueous phase. The water channel was relaxed to prevent steric overlap with the side chain.

ACKNOWLEDGMENT

We are grateful to Professor Thomas Link for providing us with the coordinates of the ISP soluble fragment before these were publicly available. The crystallographic work was partially done at SSRL which is operated by the Department of Energy, Division of Chemical/Material Sciences. The SSRL Biotechnology Program is supported by the National Institutes of Health Biomedical Resource Technology Program, Division of Research Resources. We acknowledge help with EPR spectra of mutant strains that were measured by Dr. H. Ding in the laboratory of Professor P. L. Dutton.

REFERENCES

1. Gennis, R. B., Barquera, B., Hacker, B., van Doren, S. R., Arnaud, S., Crofts, A. R., Davidson, E., Gray, K. A., and Daldal, F. (1993) *J. Bioenerg. Biomembr. 25*, 195−210.
2. Brandt, U., and Trumpower, B. L. (1994) *CRC Crit. Rev. Biochem. 29*, 165−197.
3. Degli Esposti, M., De Vries, S., Crimi, M., Ghelli, A., Patarnello, T., and Meyer, A. (1993) *Biochim. Biophys. Acta 1143*, 243−271.
4. Schägger, H., Brandt, U., Gencic, S., and von Jagow, G. (1995) *Methods Enzymol. 260*, 82−96.
5. Brasseur, G., Sami Saribas, A., and Daldal, F. (1996) *Biochim. Biophys. Acta 1275*, 61−69.
6. Brandt, U. (1998) *Biochim. Biophys. Acta 1365*, 261−268.
7. Zhang, Z., Huang, L., Shulmeister, V. M., Chi, Y.-I., Kim, K. K., Hung, L.-W., Crofts, A. R., Berry, E. A., and Kim, S.-H. (1998) *Nature (London) 392*, 677−684.
8. Xia, D., Yu, C.-A., Kim, H., Xia, J.-Z., Kachurin, A. M., Zhang, L., Yu, L., and Deisenhofer, J. (1997) *Science 277*, 60−66.
9. Iwata, S., Lee, J. W., Okada, K., Lee, J. K., Iwata, M., Rasmussen, B., Link, T. A., Ramaswamy, S., and Jap, B. K. (1998) *Science 281*, 64−71.
10. Kim, H., Xia, D., Yu, C. A., Xia, J. Z., Kachurin, A. M., Zhang, L., Yu, L., and Deisenhofer, J. (1998) *Proc. Natl. Acad. Sci. U.S.A. 95*, 8026−8033.
11. Crofts, A. R., and Berry, E. A. (1998) *Curr. Opin. Struct. Biol. 8*, 501−509.
12. Andrews, K. M., Crofts, A. R., and Gennis, R. B. (1990) *Biochemistry 29*, 2645−2651.
13. Ljungdahl, P. O., Pennoyer, J. D., Robertson, D. E., and Trumpower, B. L. (1987) *Biochim. Biophys. Acta 891*, 227−241.
14. Mitchell, P. (1976) *J. Theor. Biol. 62*, 327−367.
15. Crofts, A. R., Meinhardt, S. W., Jones, K. R., and Snozzi, M. (1983) *Biochim. Biophys. Acta 723*, 202−218.
16. Meinhardt, S. W., and Crofts, A. R. (1983) *Biochim. Biophys. Acta 723*, 219−230.
17. Crofts, A. R., and Wraight, C. A. (1983) *Biochim. Biophys. Acta 726*, 149−186.
18. Glaser, E. G., and Crofts, A. R. (1984) *Biochim. Biophys. Acta 766*, 322−333.
19. Crofts, A. R. (1985) in *The Enzymes of Biological Membranes* (Martonosi, A. N., Ed.) Vol. 4, pp 347−382, Plenum, New York.
20. Robertson, D. E., and Dutton, P. L. (1988) *Biochim. Biophys. Acta 935*, 273−291.
21. Crofts, A. R., and Wang, Z. (1989) *Photosynth. Res. 22*, 69−87.
22. Jünemann, S., Heathcote, P., and Rich, P. (1998) *J. Biol. Chem. 273*, 21603−21607.
23. Bowyer, J. R., Dutton, P. L., Prince, R. C., and Crofts, A. R. (1980) *Biochim. Biophys. Acta 592*, 445−460.
24. Ohnishi, T., Schagger, H., Meinhardt, S. W., LoBrutto, R., Link, T. A., and von Jagow, G. (1989) *J. Biol. Chem. 264*, 735−741.
25. von Jagow, G., and Link, T. A. (1986) *Methods Enzymol. 126*, 253−271.
26. Matsuura, K., Bowyer, J. R., Ohnishi, T., and Dutton, P. L. (1983) *J. Biol. Chem. 258*, 1571−1579.
27. Meinhardt, S. W., and Crofts, A. R. (1982). *FEBS Lett. 149*, 217−222.
28. Sauter, H., Ammermann, E., and Roehl, F. (1996) in *Crop Protection Agents from Nature* (Copping, L. G., Ed.) pp 50−81, The Royal Society of Chemistry, Thomas Graham House, Cambridge, U.K.
29. Link, T. A., Haase, U., Brandt, U., and von Jagow, G. (1993) *J. Bioenerg. Biomembr. 25*, 221−232.
30. Brandt, U., Schaegger, H., and von Jagow, G. (1988) *Eur. J. Biochem. 173*, 499−506.
31. Siedow, J. N., Power, S., De La Rosa, F. F., and Palmer, G. (1978) *J. Biol. Chem. 253*, 2392−2399.
32. De Vries, S., Albracht, S. P. J., and Leeuwerik, F. J. (1979) *Biochim. Biophys. Acta 546*, 316−333.
33. De Vries, S., Albracht, S. P. J., Berden, J., and Slater, E. C. (1982) *Biochim. Biophys. Acta 681*, 41−53.
34. Ding, H., Robertson, D. E., Daldal, F., and Dutton, P. L. (1992) *Biochemistry 31*, 3144−3158.
35. Ding, H., Moser, C. C., Robertson, D. E., Tokito, M. K., Daldal, F., and Dutton, P. L. (1995) *Biochemistry 34*, 15979−15996.
36. Ding, H., Daldal, F., and Dutton, P. L. (1995) *Biochemistry 34*, 15997−16003.
37. Saribas, A. S., Ding, H. G., Dutton, P. L., and Daldal, F. (1997) *Biochim. Biophys. Acta 1319*, 99−108.
38. Crofts, A. R., Guergova-Kuras, M., Huang, L.-S., Kuras, R., Zhang, Z., and Berry, E. A. (1999) Mechanism of ubiquinol oxidation by the bc_1 complex: role of the iron sulfur protein and its mobility. *Biochemistry 38*, 15791−15806.
39. Crofts, A. R., Hong, S., Zhang, Z., and Berry, E. A. (1999) Physicochemical aspects of the movement of the Rieske iron sulfur protein during quinol oxidation by the bc_1 complex from mitochondria and photosynthetic bacteria, *Biochemistry 38*, 15827−15839.
40. Crofts, A. R., Barquera, B., Gennis, R. B., Kuras, R., Guergova-Kuras, M., and Berry, E. A. (1999) In *The Phototrophic Prokaryotes* (Peschek, G. A., Loeffelhardt, W., and Schmetterer, G., Eds.) pp 229−239, Plenum, New York.
41. Ugulava, N., and Crofts, A. R. (1998) *FEBS Lett. 440*, 409−413.
42. Crofts, A. R., Berry, E. A., Kuras, R., Guergova-Kuras, M., Hong, S., and Ugulava, N. (1998) in *Photosynthesis: Mechanisms and Effects* (Garab, G., Ed.). Vol. III, pp 1481−1486. Kluwer Academic Publishers, Dordrecht, The Netherlands.
43. Crofts, A. R., Barquera, B., Bechmann, G., Guergova, M, Salcedo-Hernandez, R., Hacker, B., Hong, S., and Gennis, R. B. (1995) in *Photosynthesis: from light to biosphere* (Mathis, P., Ed.) Vol. II, pp 493−500. Kluwer Academic Publishers, Dordrecht, The Netherlands.
44. Yun, C.-H., Beci, R., Crofts, A. R., Kaplan, S., and Gennis, R. B. (1990) *Eur. J. Biochem. 194*, 399−411.
45. Sali, A., and Blundell, T. L. (1993) *J. Mol Biol. 234*, 779−815.
46. Surles, M., Richardson, J., Richardson, D., and Brooks, F. (1994) *Protein Sci. 3*, 198−210.
47. Izrailev, S., Crofts, A. R., Berry, E. A., and Schulten. K. (1999) *Biophys. J. 77*, 1753−1768.
48. Crofts, A. R., Hacker, B., Barquera, B., Yun, C.-H., and Gennis, R. (1992) *Biochim. Biophys. Acta 1101*, 162−165.
49. Crofts, A. R., Hong, S., Ugulava, N., Barquera, B., Gennis, R., Guergova-Kuras, M. and Berry, E. A. (1999) *Proc. Natl. Acad. Sci. U.S.A. 96*, 10021−10026.
50. Snozzi, M., and Crofts, A. R. (1984) *Biochim. Biophys. Acta 766*, 451−463.
51. Venturoli, G., Fernandez-Velasco, J. G., Crofts, A. R., and Melandri, B. A. (1988) *Biochim. Biophys. Acta 935*, 258−272.
52. Brandt, U. (1996) *Biochim. Biophys. Acta 1275*, 41−46.
53. Brandt, U. (1996) *FEBS Lett. 387*, 1−6.
54. Brandt, U., and Okun, J. G. (1997) *Biochemistry 36*, 11234−11240.

55. Gopta, O. A., Feniouk, B. A., Junge, W. and Mulkidjanian, A. Y. (1998) *FEBS Lett. 431*, 291−296.
56. Link, T. A. (1997) *FEBS Lett. 412*, 257−264.
57. Skulachev, V. P. (1996) *Q. Rev. Biophys. 29*, 169−202.
58. Chen, Y., and Crofts, A. R. (1990) in *Current Research in Photosynthesis* (Baltscheffsky, M., Ed.) Vol. III, pp 287−290. Kluwer Academic Publishers, Dordrecht, The Netherlands.
59. Iwata, S., Saynovits, M., Link, T. A., and Michel, H. (1996) *Structure 4*, 567−579.
60. Crofts, A. R., Guergova-Kuras, M., and Hong, S. (1998) *Photosynth. Res. 55*, 357−362.
61. Lancaster, C. R., and Michel, H. (1997) *Structure 5*, 1339−1359.
62. Brandt, U., and von Jagow, G. (1991) *Eur. J. Biochem. 195*, 163−170.
63. Stowell, M. H. B., McPhillips, T. M., Rees, D. C., Soltis, S. M., Abresch, E., and Feher, G. (1997) *Science 276*, 812−815.
64. Andrews, K. (1988) Ph.D. Thesis, University of Illinois, Urbana, IL.
65. Moser, C. C., Page, C. C., Farid, R. and Dutton, P. L. (1995) *J. Bioenerg. Biomembr. 27*, 263−274.
66. DeVault, D. (1980) *Q. Rev. Biophys. 13*, 387−564.
67. Hong, S., Ugulava, N., Guergova-Kuras, M., and Crofts, A. R. (1999) *J. Biol. Chem.* (in press).

BI990962M